Published in final edited form as:
Q J Nucl Med Mol Imaging. 2010 June ; 54(3): 291–308.

Preclinical Molecular Imaging of Tumor Angiogenesis

Lei Zhu[1,2], **Gang Niu**[1,3], **Xuexun Fang**[2], and **Xiaoyuan Chen**[1]

[1] Laboratory of Molecular Imaging and Nanomedicine (LOMIN), National Institute of Biomedical Imaging and Bioengineering (NIBIB), National Institutes of Health (NIH), Bethesda, MD 20892-2281, USA

[2] College of Life Science, Jilin University, Changchun 130012, P.R. China

[3] Imaging Sciences Training Program, Radiology and Imaging Sciences, Clinical Center and National Institute Biomedical Imaging and Bioengineering, NIH, 20892, USA

Abstract

Angiogenesis, a course that new blood vessels grow from the existing vasculature, plays important roles both physiologically and pathologically. Angiogenesis can be switched on by growth factors secreted by tumor cells, and in turn supplies more oxygen and nutrition to the tumor. More and more preclinical studies and clinical trials have shown that inhibition of angiogenesis is an effective way to inhibit tumor growth, substantiating the development of anti-angiogenesis therapeutics. Imaging technologies accelerate the translation of preclinical research to the clinic. In oncology, various imaging modalities are widely applied to drug development, tumor early detection and therapy response monitoring. So far, several angiogenesis related imaging agents are promising in cancer diagnosis. However, more effective imaging agents with less side-effect still need to be pursued to visualize angiogenesis process non-invasively. The main purpose of this review is to summarize the recent progresses in preclinical molecular imaging of angiogenesis and to discuss the potential of the current preclinical probes specific to various angiogenesis targets including vascular endothelial growth factor and its receptors (VEGF/VEGFRs), integrin $\alpha_v\beta_3$ and matrix metalloproteinases (MMPs). It is predicable that related investigations in the field will benefit cancer research and quicken the anti-angiogenic drug development.

Keywords

angiogenesis; molecular imaging; vascular endothelial growth factor receptor; integrin $\alpha_v\beta_3$; matrix metalloproteinases

INTRODUCTION OF TUMOR ANGIOGENESIS

Angiogenesis is critical in both physiological development and pathological processes such as tumor progression, wound healing, cardiovascular, inflammatory, ischemic, and infectious diseases [1–3]. For multicellular tumor clones to grow beyond 100–200 μm, they must recruit new blood vessels by angiogenesis and vasculogenesis [4–6]. It is now widely accepted that both mutations of oncogenes and tumor suppressor genes lead to the switch into an angiogenic tumor, i.e., the endogenous balance between pro-angiogenic and anti-

Correspondence: Dr. Xiaoyuan Chen, Laboratory of Molecular Imaging and Nanomedicine (LOMIN), National Institute of Biomedical Imaging and Bioengineering (NIBIB), National Institutes of Health (NIH), 31 Center Drive, Suite 1C14, Bethesda, MD 20892-2281, shawn.chen@nih.gov. Gang Niu, PhD, Laboratory of Molecular Imaging and Nanomedicine (LOMIN), National Institute of Biomedical Imaging and Bioengineering (NIBIB), National Institutes of Health (NIH), 9 Memorial Drive, 9/1W111, Bethesda, MD 20892, niug@mail.nih.gov.

angiogenic molecules is tipped in favor of angiogenesis [7–9]. For example, tumor tissues produce and release angiogenic growth factors such as vasculoendothelial growth factor (VEGF), the acidic and basic fibroblast growth factors (aFGF, bFGF), and the platelet-derived endothelial cell growth factor (PD-ECGF) [10]. When these angiogenic growth factors bind to their corresponding specific receptors located on the endothelial cells of pre-existing blood vessels, various signal transduction pathways are activated to promote the activation of endothelial cells [11,12]. Subsequently, the original vessels undergo characteristic morphological changes, including enlargement of the diameter, basement membrane degradation, a thinned endothelial cell lining, increased endothelial number, decreased number of pericytes and detachment of pericytes [13]. Tumor angiogenesis also involves an intricate interplay between the tumor and surrounding or supportive cells, including vascular endothelial cells, pericytes, smooth muscle cells, fibroblasts and tumor-associated macrophages [14]. Tumor vessels can grow by several different patterns including sprouting, intussusception or incorporation of bone marrow-derived endothelial precursors. In addition, tumor cells can co-opt existing vessels [15]. Sprouting angiogenesis is the most important mechanism for tumor vascularization, which involves several steps from the growth of endothelial sprouts from preexisting post-capillary venules to the growth and remodeling process of the primitive network into a complex network [2,16–18].

At the sprouting tips of growing vessels, endothelial cells secrete matrix metalloproteinases (MMPs) to facilitate the degradation of extracellular matrix and cell invasion [19]. Cell surface adhesion molecules such as integrins also play an important role in endothelial cell migration and in contact with the extracellular tumor matrix, facilitating cell survival [20,21]. Next, a lumen within an endothelial cell tubule has to be formed, which requires interactions between the extracellular matrix and cell-associated surface proteins, such as galectin-2, PECAM-1, and VE-cadherin [22]. Finally, newly formed vessels are stabilized through the recruitment of smooth muscle cells and pericytes. Unlike blood vessels in healthy tissues, the tumor vasculatures appear as disorganized tubular structures, which are often interconnected, tortuous, highly leaky, resembling premature sinusoidal vasculatures [23,24]. These abnormal vessels usually lack a clear separation between arterioles and venules and the recruitment of pericytes and vascular smooth muscle cells [25].

IMAGING OF TUMOR ANGIOGENSIS

Anti-angiogenesis therapy and tumor response assessment

In as early as 1971, Folkman proposed that anti-angiogenesis might be an effective anticancer strategy [6] based on the observation that tumor growth was associated with marked vascularity [26]. Recognition of the VEGF pathway as a key regulator of angiogenesis has led to the development of several VEGF-targeted agents, including agents that prevent VEGF-A from binding to its receptors [27], antibodies that directly block VEGFR-2 [28,29], and small molecules that inhibit the kinase activity of VEGFR-2 thereby blocking growth factor signaling [30–32]. Many studies using VEGF-targeted therapies in murine models demonstrated that inhibition of VEGF signaling could lead to tumor endothelial cell apoptosis, although rarely did such therapies lead to regression of established tumors [33,34].

So far, hundreds of molecules with anti-angiogenic activity in preclinical models have been reported, and many of them have entered clinical testing in oncology. Several of them have been approved for human use in solid tumors. For example, Bevacizumab, a monoclonal antibody against VEGF-A, is the first clinically available angiogenesis inhibitor in US [35]. Another category of VEGF/VEGFR targeted therapeutics is tyrosine kinase inhibitors. These agents compete with ATP for binding within the intracellular domain of various wild-type and/or mutated receptor tyrosine kinases [36]. Unlike Bevacizumab, which targets

extracellular VEGF, tyrosine kinase inhibitors target the intracellular signaling pathways of VEGFRs [37].

The most commonly used end-point for assessing anti-angiogenic treatment in clinical studies is microvessel density (MVD), measured from biopsies taken before and at one or more times after treatment, using a variety of immunohistochemical vascular markers such as CD34, CD31, CD105 and von Willebrand factor (vWF) to identify the vessels [38]. However, measurement of MVD is problematic for assessing the vascular efficacy of antiangiogenic agents [39] since blocking angiogenesis may be accompanied by a proportional reduction in tumor growth that would not result in a net change in MVD. Besides, vessel counts and/or density may remain unchanged even in the face of effective therapy [40]. Therefore, although a reduction in MVD following treatment is indicative of an antiangiogenic effect, it does not mean that no change in MVD is indicative of no antiangiogenic effect, as is commonly assumed.

Non-invasive imaging methods for measuring functional vascular volume are available and can provide a noninvasive means of detecting angiogenesis within and about the perimeter of the whole tumor and give functional information. For instance, PET studies with ^{15}O-oxygen and related tracers can offer direct physiological measurement of circulatory parameters of regional blood flow and vascular volume [41]. Ultrasound (particularly microbubble contrast enhanced ultrasound) is also a valuable imaging modality to determine the tumor microvascular blood volume and blood velocity [42]. Especially, dynamic contrast-enhanced ultrasonography (DCE-US) allows repeated examinations and provides both morphologic and functional analyses. Several quantitative parameters considered as indicators of tumor flow such as the peak intensity (PI) or time-to-PI can be extracted from the time-intensity curves of contrast uptake [43]. Power Doppler ultrasonography has been used to demonstrate the presence of blood flow in small vessels and it was also found that the vascular signal correlates with histopathological quantification of the vascular density of synovial tissue [44].

Dynamic contrast-enhanced MRI (DCE-MRI) has also been well established to investigate angiogenesis within tumors, and in particular the response to antiangiogenic therapy. The leakage of MR contrast agent through tumor vessels results in a fast “wash-in” of contrast coupled with the rapid “wash-out,” and allows a functional analysis of the tumor microcirculation [45]. DCE-MRI has been the most utilized pharmacodynamic imaging modality in early phase clinical trials of angiogenic inhibitors. This functional imaging technique is non-invasive and can be used to serially assess tumor vasculature *in vivo* [46]. However, like MVD measurements, a negative effect on vascular volume indicated by non-invasive imaging cannot be interpreted as absence of antiangiogenic effect, either [47]. Indeed, a study in a xenograft model of human breast cancer showed a poor correlation between MVD and fractional blood volume estimates as measured by functional MRI and macromolecular contrast agents [34]. Tumor blood flow rate is also an accessible end-point for clinical studies. A decrease in tumor blood flow rate is expected if MVD is decreased and its measurement would provide additional functional information linked to oxygen availability and tumor growth. However, some pre-clinical studies have demonstrated an increase in tumor blood flow rate following antiangiogenic therapy. For example, Teicher et al. [48] showed that tumor blood flow and oxygenation significantly was increased in the first weeks of treatment with TNP-470, a synthetic analogue of fumagillon. Following antiangiogenic therapy, blood flow rate within individual vessels may be improved, which has been termed as “normalizing tumor vasculature” [49]. The mechanisms may lie in that the most immature and inefficient tumor blood vessels are “pruned” from the tumor vascular network by antiangiogenic therapy, leaving a more efficient system [49]. In addition, many pro-angiogenic growth factors are associated with high vascular permeability and their withdrawal can

reverse this effect [50]. It is possible that a decrease in vascular permeability to macromolecules could improve blood flow rate by reducing tumor interstitial fluid pressure. Thus, measurement of vascular permeability or interstitial fluid pressure could provide alternative end-points for assessing tumor vascular effects of antiangiogenic agents [47].

Molecular imaging of tumor angiogenesis

Compared with traditional method, molecular imaging usually exploits specific molecular probes as well as intrinsic tissue characteristics as the source of imaging contrast, and provides the potential for understanding the integrative biology, earlier detection and characterization of disease, and evaluation of treatment [51]. Imaging probes with high affinity and specificity would be the key to successful molecular imaging. Currently, several important angiogenesis related targets including VEGF/VEGFRs, integrins, and MMPS are being intensively investigated to evaluate both tumor angiogenesis and tumor response to various anti-angiogenesis drugs.

Imaging VEGF/VEGFRs—In view of the critical role of VEGF/VEGFR in cancer progression, development of VEGF- or VEGFR-targeted molecular imaging probes could serve as a new paradigm for the assessment of anti-angiogenic therapeutics, and for better understanding the role and expression profile of VEGF/VEGFR in many angiogenesis-related diseases. Due to the soluble and more dynamic nature of VEGF, imaging VEGF expression and explanation of the imaging results can be difficult, although single photon emission computed tomography (SPECT) or positron emission tomography (PET) imaging of VEGF has been performed with radiolabeled anti-VEGF antibodies [52]. VG76e, an IgG_1 monoclonal antibody that binds to human VEGF, was labeled with ^{124}I for PET imaging of solid tumor xenografts in immune-deficient mice [53]. Whole-animal PET imaging studies revealed a high tumor-to-background contrast. Although VEGF specificity *in vivo* was demonstrated in this report, the poor immunoreactivity (< 35%) of the radiolabeled antibody limits the potential use of this tracer. HuMV833, the humanized version of a mouse monoclonal anti-VEGF antibody MV833, was also labeled with ^{124}I and the distribution and biological effects of HuMV833 in patients in a phase I clinical trial were investigated [54]. Patients with progressive solid tumors were treated with various doses of HuMV833 and PET imaging using ^{124}I-HuMV833 was carried out to measure the antibody distribution in and clearance from tissues. It was found that antibody distribution and clearance were quite heterogeneous not only between and within patients but also between and within individual tumors. Bevacizumab, a humanized monoclonal antibody against VEGF, has been labeled with ^{111}In to image VEGF-A expression in nude mice model or patients with colorectal liver metastases [55]. Although enhanced uptake of ^{111}In-bevacizumab in the liver metastases was observed in 9 of the 12 patients, there was no correlation between the level of ^{111}In-antibody accumulation and the level of VEGF-A expression in the tissue as determined by in situ hybridization and ELISA [55]. Bevacizumab has also been labeled with the PET isotope ^{89}Zr for noninvasive in vivo VEGF visualization and quantification. On small-animal PET images, radiolabeled bevacizumab showed higher uptake compared with radiolabeled human IgG in a human SKOV-3 ovarian tumor xenograft. Tracer uptake in other organs was seen primarily in the liver and spleen (Figure 1) [52]. However, the slow distribution and clearance of antibodies within tumors also make it not an optimal tracer to monitor therapy response of tumors to anti-angiogenic treatment.

The more rational design is to use radiolabeled VEGF isoforms for SPECT or PET imaging of VEGFR expression. With SPECT imaging, recombinant human $VEGF_{121}$ was labeled with ^{111}In for the identification of ischemic tissue in a rabbit model, where unilateral hind-limb ischemia was created by femoral artery excision [18]. $VEGF_{121}$ has also been labeled with ^{99m}Tc through an “Adapter/Docking” strategy and the tracer was tested in a murine

mammary carcinoma [56]. Cai *et al.* have labeled $VEGF_{121}$ with ^{64}Cu for PET imaging of tumor angiogenesis and VEGFR expression [57]. MicroPET imaging revealed the dynamic nature of VEGFR expression during tumor progression in that even for the same tumor model, VEGFR expression level can be dramatically different at different stages. Indeed, the uptake of ^{64}Cu-DOTA-$VEGF_{121}$ in the tumor peaked when the tumor size was about 100–250 mm^3. Both small and large tumors had lower tracer uptake indicating a narrow range of tumor size with high VEGFR-2 expression. The tumor uptake value obtained from PET imaging had good linear correlation with the relative tumor tissue VEGFR-2 expression as measured by Western blot [58].

Random radiolabeling or bioconjugation may impair VEGF conformation and result in high uptake in major organs, such as liver and kidney [59]. Modification of the protein at a specific site or using a linker can avoid impairing the structure of VEGF. Blankenberg *et al.* constructed recombinant VEGF containing a cysteine containing peptide tag (C-tag) that allows for site-specific modification of C-tag-containing fusion proteins with a bifunctional chelator, HYNIC (hydrazine nicotinamide)-maleimide [60]. With ^{99m}Tc labeled HYNIC-VEGF, 4T1 murine breast tumors showed a decreased contrast agent uptake after treatment. In the following study, a new single-chain Cys-tagged VEGF (scVEGF) was developed by fusion of two fragments (amino acids 3–112) of human $VEGF_{121}$ [56]. The scVEGF showed a high binding affinity to VEGFR-2 and receptor mediated internalization into PAE/KDR cells. After being conjugated with Cy dye molecule, ^{99m}Tc and ^{64}Cu, *in vivo* imaging indicated that all the tumors showed enhanced contrast agent uptake by the optical, SPECT and PET imaging. We developed an alternative site-specific modification of VEGF with an Avi-tag fused to the C-terminus of $VEGF_{121}$ to allow site-specific biotinylation without disruption of $VEGF_{121}$ function [61]. The biotinylated $VEGF_{121}$-Avi (VEGF-Avib) was able to form a stable complex with streptavidin-IRDy800 (SA800). VEGF-Avib/SA800 had significantly higher tumor signal intensity in a 67NR murine breast cancer xenograft model. Tumor-to-background ratio was higher than those of randomly labeled control $VEGF_{121}$ probes at all different times up to 66 hours, confirming the superiority of site-specific labeling strategy (Figure 2).

It is well known that all VEGF-A isoforms bind to both VEGFR-1 and VEGFR-2. A VEGFR-2-specific PET tracer has been developed using the D63AE64AE67A mutant of $VEGF_{121}$ ($VEGF_{DEE}$) generated by recombinant DNA technology. The renal uptake of ^{64}Cu-DOTA-$VEGF_{DEE}$ was significantly lower than that of ^{64}Cu-DOTA-$VEGF_{121}$ as rodent kidneys expressed high levels of VEGFR-1 based on immunofluorescence staining [62]. With the development of new tracers with better targeting efficacy and desirable pharmacokinetics, clinical translation will be critical for the maximum benefit of VEGF-based imaging agents. Peptidic VEGFR antagonists can be labeled with short-lived isotopes such as ^{18}F and they may allow for higher throughput than antibody- or protein-based radiotracers, as one hour post-injection is usually sufficient for a peptide-based tracer to clear from the non-targeted organs and give high contrast images [63]. One peptide (QKRKRKKSRYKS) encoded by $VEGF\text{-}A_{189}$ exon 6 was reported [64] and labeled with ^{188}Re for SPECT imaging of VEGFR in tumor-bearing nude mice. Planar imaging with SPECT demonstrated significant radioactivity accumulation in tumor 1 h after injection of the labeled peptide and disappearance of radioactivity 3 h later, facilitating repetitive imaging with the peptide for therapy response monitoring [65].

Ultrasonography (US) is by far one of the most commonly used clinical imaging modalities because it is safe and cost effective. Ultrasonic contrast agents such as microbubbles have been the subject of active research, especially in recent years, with added interest in developing site-directed ultrasonic contrast agents [51]. With at least several micrometers in diameter, microbubbles are too large to extravasate so only the tumor endothelium can be

targeted [66]. Moreover, acoustic destruction of "payload-bearing" microbubbles can be used to deliver drugs or to augment gene transfection [67]. Angiogenesis-targeted microbubbles may also have applications in site-specific therapy for ischemic tissues or tumors. Thus, VEGFR-2 is an excellent candidate for targeted untrasound imaging since it is almost exclusively expressed on activated endothelial cells [68]. In a mouse model of pancreatic adenocarcinoma, anti-VEGFR2 or anti VEGF-VEGFR complex antibodies conjugated microbubbles were used to image and quantify vascular effects of two different anti-tumor therapies in both subcutaneous and orthotopic pancreatic tumors [66]. Significant signal enhancement of tumor vasculature was observed when compared with untargeted or control IgG-targeted microbubbles. Video intensity from targeted microbubbles also correlated with the expression level of the target (VEGFR-2 or the VEGF-VEGFR complex) and with MVD in tumors under therapy. In another report, Willmann *et al.* have imaged VEGFR-2 expression in two murine tumor models using anti-VEGFR2 monoclonal antibody conjugated microbubbles [69,70]. Contrast-enhanced ultrasound imaging using targeted microbubbles showed significantly higher average video intensity compared with control microbubbles in both tumor models. These studies support that targeted microbubbles can be used for non-invasive, vascularture-targeted molecular imaging of tumor angiogenesis and for *in vivo* monitoring of vascular effects after therapy. Recently, BR55, an ultrasound contrast agent was evaluated *in vitro* and *in vivo* for the molecular imaging of tumoral angiogenesis [71]. BR55 was based on a heterodimer peptide targeting the VEGFR2, and incorporation of a biospecific lipopeptide into the microbubble membrane. BR55 showed a similar accumulation in tumor as microbubble bearing the specific antibody. In the meantime, Pillai *et al.* attached a heterodimeric peptide to a pegylated phospholipid and showed that the resulting construct retained nanomolar affinity for its target, VEGFR-2. They demonstrated that the phospholipid-PEG2000-peptide is smoothly incorporated into gas-filled microbubbles and provides imaging of angiogenesis in a rat tumor model [72].

Although optical imaging may not be widely used in clinical settings, near infrared (NIR) (700–900 nm) approaches provide opportunities for rapid and cost-effective preclinical evaluation in small animal models. Optical imaging has been used to study gene expression [73], tumor angiogenesis, physiological function of tumors, and tumor metastasis [74]. In a transgenic mouse model where a VEGF promoter was chosen to drive a GFP reporter gene, VEGF expression during wound healing and possible impairment of wound healing due to collateral tissue damage was imaged *in vivo* [73]. Human VEGF has also been conjugated to a self-assembled "dock and lock" system and retained its functional activities [75]. After incorporating an additional cysteine residue for site-specific modification, a NIR fluorescent dye Cy5.5 (maximum emission 696 nm) was conjugated and the resulting Cy5.5-VEGF was used for *in vivo* imaging. Although tumor contrast was observed after administration of the probe, no information was reported about the whole body distribution of Cy5.5-VEGF [75,76]. To develop a dual-function PET/NIRF probe, our group conjugated VEGF protein and DOTA chelator on an amine-functionalized QD (DOTA-QD-VEGF) for VEGFR-targeted PET/NIRF imaging. The DOTA-QD-VEGF exhibited VEGFR-specific binding in both cell-binding assay and cell staining experiment. Both NIR fluorescence imaging and microPET showed VEGFR-specific delivery of conjugated DOTA-QD-VEGF nanoparticle and prominent reticuloendothelial system uptake. Moreover, good correlation was also observed between the results measured by *ex vivo* PET and NIRF organ imaging [77]. Another component of optical imaging is bioluminescence imaging (BLI), which can be used to detect very low levels of signal because the emitted light is virtually background free [78]. Non-invasive indirect imaging of VEGF expression with BLI in living transgenic mice has also been reported, where a two-step transcriptional amplification approach was used to augment the transcriptional activity of the relatively weak VEGF promoter [79].

Imaging of integrins—Integrins are a family of receptors comprised of a family of heterodimeric glycoproteins, which are involved in the formation of new blood vessels in tumors [80]. Integrins expressed on endothelial cells are related to cell survival and migration during angiogenesis, while integrins expressed on carcinoma cells modulate metastasis by facilitating invasion and movement across the vessels [81]. Each integrin member consists of an α and a β subunit, 18 different α and 8 different β subunits are known in mammals, which can combine to 24 different integrin receptors [82,83]. Among them, the $\alpha_v\beta_3$ integrin, which binds to arginine-glycine-aspartic acid (RGD)-containing components of the interstitial matrix such as vitronectin, fibronectin and thrombospondin [84,85], is expressed in a number of tumor types such as melanoma, late stage glioblastoma, ovarian, breast, and prostate cancer [63,86,87]. Integrin $\alpha_v\beta_3$ promotes angiogenesis and endothelial cell survival and that antagonism of this integrin suppresses angiogenesis by inducing endothelial cell apoptosis *in vitro* and *in vivo* [80,88,89]. Apart from $\alpha_v\beta_3$, integrin $\alpha_v\beta_1$, $\alpha_v\beta_5$, $\alpha_5\beta_1$, and $\alpha_4\beta_1$ also play important roles in regulating angiogenesis.

Integrins are ideal pharmacological targets based on both the key role they played in angiogenesis, leukocytes function and tumor development and easy accessibility as cell surface receptors interacting with extracellular ligands [90]. So far, the integrin superfamily represents the best opportunity of targeting both antibodies and small-molecule antagonists for both therapeutic and diagnostic utility in various key diseases [91]. Preclinical studies and clinical trials showed that quite a few integrin targeting antibodies were effective in blocking tumor growth and metastasis [80,92,93]. Small molecular antagonists, mainly based on RGD containing peptides and RGD peptidomimetics [94–96], also showed potent inhibition of angiogenesis. More detailed information can be found in several recently published review articles [90,97].

First *in vivo* application of radioiodinated RGD peptides revealed the receptor-specific tumor uptake but also predominantly hepatobiliary elimination, resulting in high activity concentration in the liver and small intestines [98]. Consequently, several strategies to improve the pharmacokinetics of radiohalogenated peptides have been studied including conjugation with sugar moieties, hydrophilic amino acids and polyethylene glycol (PEG) [99–102]. Besides radiohalogenated RGD peptides, a variety of radiometalated tracers have been developed as well, including peptides labeled with ^{111}In, ^{99m}Tc, ^{64}Cu, ^{90}Y, ^{188}Re and ^{68}Ga [103–106]. Most of them are based on the cyclic pentapeptide c(RGDfK) or c(RGDyK) and are conjugated via the γ-amino function of a lysine with different chelator systems, like diethylene triamine pentaacetic acid (DTPA), the tetrapeptide sequence H-Asp-Lys-Cys-Lys-OH, 1,4,7,10-tetraazacyclododecane-1,4,7,10-tetraacetic acid (DOTA) and 1,4,7-triazacyclononane-1,4,7-triacetic acid (NOTA). While all these compounds have shown high receptor affinity and selectivity and specific tumor accumulation, the pharmacokinetics of most of them still need to be improved [107]. NC100692 is a cyclic synthetic RGD containing ligand with disulfide bond. The compound ^{99m}Tc-NC100692 by GE Healthcare has been used for SPECT imaging in preclinical and clinical studies [108]. Another radiotracer, ^{18}F-AH111585 has the core sequence of ACDCRGDCFCG and was also applied to detect tumors in metastatic breast cancerpatients using PET imaging [109].

In a human melanoma M21 model, ^{18}F-Galacto-RGD showed a tumor uptake of 1.5 %ID/g at 120 min postinjection (p.i.) [110,111]. A correlation between integrin expression and tracer accumulation was observed in imaging studies with mice bearing melanoma tumors with increasing amounts of $\alpha_v\beta_3$-positive cells [112]. ^{18}F-Galacto-RGD has also been applied to patients and successfully imaged $\alpha_v\beta_3$ expression in human tumors with good tumor/background ratios [113]. Rapid clearance of ^{18}F-Galacto-RGD from the blood pool and primarily renal excretion was confirmed by following biodistribution and dosimetry studies. Background activity in lung and muscle tissue was low and the calculated effective dose is

very similar to an ^{18}F-FDG scan [114]. Standard uptake values (SUVs) and tumor/blood ratios from static emission scans at ~ 60 min. p.i. of ^{18}F-Galacto-RGD were found to correlate with the intensity of immunohistochemical staining of $\alpha_v\beta_3$ expression as well as with the microvessel density [115]. There was no obvious correlation between the tracer uptake of ^{18}F-FDG and ^{18}F-Galacto-RGD in patients with various tumors, indicating that $\alpha_v\beta_3$ expression and glucose metabolism are not closely correlated in tumor lesions and that consequently ^{18}F-FDG cannot provide similar information as ^{18}F-Galacto-RGD [116].

Within physiological ^{18}F-Galacto-RGD uptake area, such as liver, spleen and intestine, lesion identification is still problematic [117]. Therefore, multimeric RGD peptides have been developed in order to provide more effective antagonists with better targeting capability and higher cellular uptake through the integrin-dependent binding [118]. The underlying rationale is that the interaction between integrin $\alpha_v\beta_3$ and RGD-containing ECM-proteins involves multivalent binding sites with clustering of integrins. Wester and Kessler groups have synthesized a series of monomeric, dimeric, tetrameric and octameric RGD peptides. These compounds contain different numbers of c(RGDfE) peptides connected via PEG linker and lysine moieties, which are used as branching units [119,120]. We also developed a series of multimeric RGD peptides labeled with ^{18}F or ^{64}Cu for PET imaging to improve the tumor-targeting efficacy and pharmacokinetics [104,121–125]. ^{18}F-FB-E[c(RGDyK)]$_2$ (abbreviated as ^{18}F-FRGD2) showed predominantly renal excretion and almost twice as much tumor uptake in the same animal model compared with the monomeric tracer ^{18}F-FB-c(RGDyK) [121,122]. Tumor uptakes quantified by microPET scans in six tumor xenograft models correlated well with integrin $\alpha_v\beta_3$ expression level measured by SDS-PAGE autoradiography. The tetrameric RGD peptide-based tracer, ^{18}F-E[E[c(RGDfK)]$_2$]$_2$, showed significantly higher receptor binding affinity than the corresponding monomeric and dimeric RGD analogues and demonstrated rapid blood clearance, high metabolic stability, predominant renal excretion and significant receptor-mediated tumor uptake with good contrast in xenograft-bearing mice [125]. Therefore, ^{18}F-E[E[c(RGDfK)]$_2$]$_2$ is a promising agent for peptide receptor radionuclide imaging as well as targeted internal radiotherapy of integrin $\alpha_v\beta_3$ positive tumors. Compared with tetramer, RGD octamer further increased the integrin avidityby another 3-fold. *In vivo* microPET imaging showed that ^{64}Cu-DOTA-RGD octamer had slightly higher initial tumor uptake and much longer tumor retention in U87MG tumor that express high level of integrin [126]. However, higher renal uptake of the octamer was also observed, which was attributed mainly to the integrin positivity of the kidneys. Several novel dimeric RGD also have been developed by insertion a Gly(3) or PEG(4) linkers between two RGD monomers.[127,128]^{18}F labeled PEG$_4$-E[PEG$_4$-c(RGDfK)]$_2$ wasnamed as ^{18}F-FP-P-PRGD$_2$. MicroPET imaging with ^{18}F-FP-P-PRGD$_2$ revealed high tumor contrast and low background in tumor-bearing nude mice (Figure 3). Biodistribution studies confirmed the *in vivo* integrin αvβ3-binding specificity of ^{18}F-FP-P-RGD$_2$ [129]. Initial studies in healthy volunteers have been tested and further clinical trials of this dimeric RGD peptide tracer on currently inderway.

Besides RGD peptides, *in vivo* imaging using Abegrin, a humanized monoclonal antibody against human integrin $\alpha_v\beta_3$, has been performed after DOTA conjugation and ^{64}Cu labeling. MicroPET studies revealed that ^{64}Cu-DOTA-Abegrin had a very high tumor activity accumulation in integrin $\alpha_v\beta_3$ positive U87MG tumors [130]. Knottins are small constrained polypeptides that share a common disulfide-bonded framework and a triple-stranded β-sheet fold [131]. Using yeast surface display screening, Kimura *et al*. [132] identified RGD containing knottin peptides with high binding affinity to $\alpha_v\beta_3$, $\alpha_v\beta_5$, and $\alpha_5\beta_1$ integrins (IC_{50} = 10–30 nM). The integrin binding knottin peptides were labeled with ^{64}Cu, ^{18}F or Cy5.5 for integrin imaging in tumor models. Compared with c(RGDfk), higher tumor uptake and lower liver uptake of integrin-binding knottins were observed in both PET and optical images [133]. The same group also developed a dual-labeled integrin-binding knottin peptides

for PET and near-infrared fluorescence imaging of integrin expression on a U87MG tumor model (Figure 4) [134]. However, further investigation is still needed to claim the superiority of these RGD-containing knottin peptides to monoric and multimeric RGD peptides.

Integrin $\alpha_v\beta_3$ has also been investigated as an imaging target using nanoparticle-based tracers. However, the main purpose of these studies is not to evaluate receptor expression levels, but to provide guidance for integrin targeted drug delivery or therapy, which is a little different from previously described peptide- or antibody- based imaging. Cai *et al.* [135] developed a quantum dot (QD)-based probe for both NIRF and PET imaging. QD surface modification with RGD peptides allows for integrin $\alpha_v\beta_3$ targeting and DOTA conjugation enables PET imaging after ^{64}Cu-labeling. Using this dual-modality probe, it was found that the majority of the probe in the tumor was within the tumor vasculature. Further observation with an intravital microscopy confirmed that RGD-QD does not extravasate. With a subcellular (approximately 0.5 μm) resolution, RGD-QD was found only bind as aggregates rather than individually [136].

Besides evaluating the functional properties of tumor vasculature, several targeted MRI contrast agents have been reported to image integrin $\alpha_v\beta_3$ after conjugation of iron oxide nanoparticles with RGD peptide. To develop a bifunctional iron oxide (IO) nanoparticle probe for PET and MRI scans of tumor integrin $\alpha_v\beta_3$ expression, RGD peptides were coupled to the surface of polyaspartic acid (PASP)-coated IO nanoparticles (RGD-PASP-IO). Both small-animal PET and T2-weighted MRI show integrin-specific delivery of conjugated RGD-PASP-IO nanoparticles and prominent reticuloendothelial system uptake [137]. In another study, Xie *et al.* synthesized ultrasmall c(RGDyK) peptide-coated IONPs (<10 nm in hydrodynamic diameter) and demonstrated their *in vivo* tumor-specific targeting capability [138]. Recently, IONPs were coated with a PEGylated amphiphilic triblock copolymer, making them water soluble and function-extendable. These particles were then conjugated with IRDye800 and c(RGDyK) for integrin $\alpha_v\beta_3$ targeting. Successful tumor homing *in vivo* was perceived in a subcutaneous U87MG glioblastoma xenograft model by both magnetic resonance imaging (MRI) and NIRF imaging [139].

Targeted ultrasound contrast agents significantly and selectively enhance the detection of a targeted vasculature. Integrin $\alpha_v\beta_3$ targeted ultrasonic contrast agents were prepared by incorporation either cyclic analogs of RGD peptide or the anti-$\alpha_v\beta_3$ antibody LM609 into microbubbles. Acoustic studies illustrate a backscatter amplitude increase from monolayers exposed to the targeted contrast agents of up to 13-fold (22 dB) relative to enhancement due to control bubbles. In addition, a linear dependence between the echo amplitude and bubble concentration was observed for bound agents [140]. Recently, the above mentioned integrin-binding knottin peptide was attached to the shell of perfluorocarbon-filled microbubbles (named as MB-Knottin$_{Integrin}$) for contrast-enhanced ultrasound imaging. *In vivo* ultrasound imaging signal was significantly enhanced after the administration of MB-Knottin$_{Integrin}$ than after the administration of control peptides.[141]

Imaging of matrix metalloproteinases—Matrix metalloproteinases (MMPs) are a family of zinc- and calcium-dependent endopeptidases which are responsible for the enzymatic degradation of connective tissue, and thus facilitate endothelial cell migration during angiogenesis [142]. In addition, MMPs process and release bioactive molecules such as growth factors, proteinase inhibitors, cytokines and chemokines [143]. Based on the different substrates specificity, MMPs family can be classified as collagenase (MMP-1, -8, -13, and -18), gelatinase (MMP-2 and -9), stromelysin (MMP-3, -10, and -11), matrilysin (MMP-7 and -26), while the other MMPs like MMP-12, -19, -20, -23, -27 and MMP-28 were not well characterized till now. Most MMPs are of secreted type while a few members (such as

membrane-type (MT) MMPs) anchor to the cell membrane either with the type I transmembrane domain or a glycosylphosphatidylinositol (GPI) linkage [144,145].

MMPs play an important role in new blood vessel formation [146–148]. Many strategies have been developed to image MMP levels for the assessment of angiogenesis [149,150]. One of them is called “smart probes” which have been developed to contain fluorescent dyes and MMP cleavable sequences [151,152]. It has been reported a MMP-2-sensitive probe was activated by MMP-2 *in vitro*, producing up to an 850% increase in near-infrared fluorescent signal intensity, and MMP-2-positive tumors were easily identified as high-signal-intensity regions as early as 1 hour after intravenous injection of the MMP-2 probe [153]. Since then, various strategies have been investigated to further improve the signal magnification, tumor delivery and enzymatic activation of the activatable probes. For example, Tsien and colleagues developed an activatable cell-penetrating peptides (ACPPs) system which is composed of two strands, a Cy5-conjugated polycation (Arg; CPPs-Cy5) and a polyanion (Glu). These domains were bridged by a MMP-cleavable peptide linker. Subsequent cleavage of the linker by MMPs dissociated the inhibitory polyanions, leaving the CPPs-Cy5 free to be internalized. *In vivo*, these ACPPs probes successfully identified HT-1080 tumors overexpressing MMP-2 and -9 [154]. In addition, ACPPs can target many xenograft tumor models from different cancer sites, as well as a thoroughly studied transgenic model of spontaneous breast cancer (mouse mammary tumor virus promoter driving polyoma middle T antigen, MMTV-PyMT) with the selectivity for MMP-2 and -9. Moreover, in accord with the known local distribution of MMP activity, accumulation is strongest at the tumor-stromal interface in primary tumors and associated metastases [155]. To improve the absolute tumor fluorescence and tumor-to-background fluorescence contrast, ACPPs were conjugated to dendrimers (ACPPDs). ACPPDs were used for guiding surgery and resulted in fewer residual cancer cells left in the animal after surgery. Animals whose tumors were moved with ACPPD guidance had a long-term tumor-free survival (Figure 5) [156]. These findings implicated a novel strategy to translate these activatable probes into the clinics.

Dark quenchers, dyes with no native fluorescence, offer advantages over conventional FRET-based probes because they do not occupy the emission spectra [157]. Black hole quencher (BHQ) dyes are commercially available dark quenchers and are able to permit efficient quenching across the visible spectrum from 480 nm into the NIR through a combination of FRET and static quenching mechanisms [158]. Dark-quenched, dual-labeled peptide probes have been designed by using a NIR fluorophore and a dark quencher for imaging protease activity. An MMP-13 activatable peptide probe was designed using a combination of the known MMP-13 substrate GPLGMRGLGK and Cy5.5 and BHQ-3 [152]. BHQ-3 has maximal absorption in the 620- to 730-nm range, which can efficiently quench NIR fluorophores such as Cy5.5. The MMP-13 probe Cy5.5-GPLGMRGLGK(BHQ-3) showed a 32-fold increase in enhancement of NIR fluorescence signals after incubation with MMP-13 *in vitro*, and the fluorescent recovery of the probe was strongly inhibited in the presence of an MMP-13 inhibitor. To further improve the *in vivo* pharmacokinetics of the activatable probes, Recently, Lee *et al.* developed a self-assembled polymeric nanoparticle based MMP activatable probe [159]. The strongly quenched MMP specific NIR peptides were used as a carrier on the surface of self-assembled chitosan tumor-homing polymeric nanoparticles. The probes produced significantly lower fluorescence in the absence of MMPs or in the present of MMP inhibitor while yielded an extremely heightened fluorescence signal when cleaved by MMP-2. MMP-positive SCC7 xenograft tumor models showed high uptake of nanosensor with minimal background signals *in vivo* [159].

In another study, Zhang *et al.* [160] designed QD conjugates which were coated with 5–10 copies of streptavidin, and conjugated with biotinylated peptide ligands via the strong biotin and streptavidin binding. The biotinylated peptide ligands consisted of a transporting group

(transporter) that could transport QDs into cells, a blocking group (blocker) that could diminish the cellular uptake of QDs, and a sensing group, sandwiched between the transporter and blocker, that could be cleaved by MMP-2 and -7. After the MMP treatment, the QD-peptide conjugates could be efficiently taken up into cells [160]. The same group also developed a protease sensing nanoplatform based on QDs and bioluminescence resonance energy transfer (QD-BRET). These nanosensors consist of bioluminescent proteins as the BRET donor, quantum dots as the BRET acceptor, and MMPs substrates sandwiched between the two as a sensing group. These nanosensors can detect the MMP activity in buffers and in mouse serum with the sensitivity to a few nanograms per milliliter and secreted proteases by tumor cells [161]. However, the *in vivo* application potential of these constructs needs to be further confirmed.

Via phage display techniques, the MMP specific decapeptide H-Cys-Thr-Thr-His-Trp-Gly-Phe-Thr-leu-Cys-OH (CTT) was found and could be labeled with ^{125}I and ^{99m}Tc. However, this tracer has unfavourable characteristics for *in vivo* imaging because the metabolic stability of the compound is low and lipophilicity is high [162]. Another group labeled this peptide with ^{111}In after conjugating it with a highly hydrophilic and negatively charged chelator DTPA. A significant correlation was observed between the accumulation in the tumor as well as tumor-to-blood ratio of ^{111}In-DTPA-CTT and gelatinase activity. Moreover, ^{111}In-DTPA-CTT showed low levels of radioactivity in the liver and kidneys [163]. CTT peptide was also labeled with ^{64}Cu after DOTA conjugation for PET imaging of MMP. ^{64}Cu-DOTA-CTT inhibited hMMP-2 and mMMP-9 with similar affinity to CTT. MicroPET imaging studies showed that ^{64}Cu-DOTA-CTT was taken up by MMP-2/9-positive B16F10 murine melanoma tumors, however, the low affinity for MMP-2 and MMP-9 and *in vivo* instability of CTT-based imaging probes need to be overcome for further applications [164].

Another approach is to label small molecule MMP inhibitors (MMPIs), which are typically used as antiangiogenic drugs. In general, MMPIs possess a zinc binding group (ZBG) complexing the zinc ion of the active site and are classified into several groups owing to their lead structures [142]. Different ^{18}F and ^{11}C labeled MMPIs have been synthesized and evaluated preclinically with mixed results [165,166]. Fluorinated MMPIs based on lead structures of the broad-spectrum inhibitors *N*-hydroxy-2(R)-[[(4-methoxyphenyl)sulfonyl](benzyl)-amino]-3-methyl-butanamide (CGS 25966) and N-hydroxy-2(R)-[[(4-methoxyphenyl)sulfonyl](3-picolyl)-amino]-3-methyl-butanamide (CGS 27023A) have been synthesized and showed high *in vitro* MMP inhibition potencies for MMP-2, MMP-8, MMP-9, and MMP-13 [167]. However, *in vivo* microPET study with ^{11}C-CGS 25966 failed to demarcate MMP positive tumors [168]. A ^{11}C-labeled MMPI (2R)-2-[[4-(6-fluorohex-1-ynyl)phenyl]sulfonylamino]-3-methylbutyric acid ^{11}C-methyl ester (^{11}C-FMAME), has also been synthesized and applied to two animal models of breast cancer, MCF-7 xenograft transfected with IL-1 and MDA-MB-435 xenograft in athymic mice. Again, low tumor-to-blood and tumor-to muscle ratios of these tracers do not allow visualization of the tumors in microPET studies [165,169]. However, biodistribution study with ^{18}F-labeled similar compound, (2R)-2-[4-(6-^{18}F-Fluorohex-1-ynyl)-benzenesulfonylamino]-3-methylbutyric acid (^{18}F-SAV03), showed higher tumor uptake of the tracer than normal organs [166]. Other MMPIs have also been synthesized and labeled with ^{111}In and ^{18}F [167,170]. Nevertheless, significant improvements in tumor MMP targeting and *in vivo* pharmacokinetics are necessary before the use of MMP radiotracer imaging can be translated into the clinic. Another hindrance for MMPs imaging is the high homology between each MMP member and it is difficult to identify specific substrates to a particular MMP [171]. Moreover, most of MMPs are expressed as soluble form, which complicate both the imaging and data analysis. It is also worth of note that there is difference between pharmacokinetic requirement for therapeutic drugs and imaging tracers. When developing a therapeutic drug, the particular

tumor uptake of the drug is not emphasized if the drug showed tumor therapeutic efficacy and no side-effect to normal organs. However, for imaging tracer development, higher tumor accumulation than normal tissues is a prerequisite for clear tumor visualization.

Other angiogenesis imaging targets—Apart from VEGF/VEGFs, integrins and MMPs, more tumor angiogenes related proteins have been identified as potential imaging targets [172]. For example, fibronectin, a large glycoprotein, can be found physiologically in plasma and tissues. Extra-domain B of fibronectin (EDB), consisting of 91 amino acids, is not present in the fibronectin molecule under normal conditions, but expressed in the endometrium in the proliferative phase and some vessels of the ovaries. It is an angiogenesis marker in a variety of solid tumors. By phage display, a human antibody fragment scFv (L19) was identified and has been shown to efficiently localize on neovasculature *in vivo*. The L19 small immunoprotein (SIP) was labeled by ^{76}Br and ^{124}I for PET imaging [173,174]. Endoglin (CD105) is a cell membrane glycoprotein mainly expressed on endothelial cells and overexpressed on tumor vasculature. Gd-DTPA liposomes were conjugated with immunoglobulins and used to detect the expression of CD105 in tumor-bearing rats by MR imaging [175]. E-selectin is a cell adhesion molecule and CD antigen that expressed exclusively by activated endothelial cells. ^{111}In-labeled E-selectin antibody was used for imaging of inflamed human synovial vasculature [176]. A significant difference was observed comparing to the control group. Other angiogenesis-related biomarkers, such as angiopoietins/Tie receptors [177], and CD276 [178] are also potential targets for angiogenesis imaging.

Imaging therapy response of tumors

Monitoring tumor response to various therapeutics is one major requirement of molecular imaging. So far, assessment of anti-angiogenic treatment in clinical studies is achieved mainly by MVD measurement and non-invasive imaging methods for measuring functional vascular volume including PET studies with ^{15}O-oxygen and related tracers [41], dynamic contrast-enhanced ultrasonography (DCE-US) [42], and dynamic contrast-enhanced MRI (DCE-MRI) [45]. For example, it has been shown that DCE-MRI can detect responses to PTK/ZK (a VEGF receptor tyrosine kinase inhibitor) therapy as early as two days after therapy with significant reductions in area under gadolinium-contrast-medium curve (AUGC) [179] or permeability parameters [180], which also predict subsequent response. LMCM DCE-MRI has also shown significant reductions in permeability values in patients treated with the antivascular agents AG-013736 (an inhibitor of the VEGF, PDGF, c-Kit receptor tyrosine kinases) and SU5416 (a selective inhibitor of VEGFR-2 tyrosine kinase) activity [181].

Molecular imaging of angiogenesis related protein targets also has been reported to monitor tumor response to treatment in preclinical models. For example, tumor uptake of ^{18}F-AH111585, a disulfide bond cyclic RGD peptide, and microvessel density were assessed in human lung cancer bearing mice treated with either low-dose paclitaxel or ZD4190, a VEGFR-2 TKI. The results showed that paclitaxel therapy reduced the MVD in LLC tumor–bearing mice and resulted in significantly reduced ^{18}F-AH111585 tumor uptake. ZD4190 therapy also resulted in a significant decrease in ^{18}F-AH111585 uptake in Calu-6 tumors, compared with the vehicle control–treated Calu-6 tumors [182]. Moreover, the decreased uptake of ^{18}F-AH111585 was matched by a decrease in the tumor MVD and FDG uptake remained unchanged with low-dose paclitaxel treatment. Another application is for the Src family kinases (SFK) inhibitor dasatinib treated U87MG xenografts bearing mice. Dasatinib significantly reduced ^{64}Cu-DOTA-c(RGDfK) uptake by up to 59% in U87MG xenografts. In contrast, tumor FDG uptake showed no significant reduction with dasatinib therapy, indicating that ^{64}Cu-DOTA-c(RGDfK) may provide a sensitive means of monitoring tumor response to SFK inhibition in $\alpha_v\beta_3$ expressing cancers in the early course of therapy [183].

Blankenberg *et al* applied ^{99m}Tc-scVEGF in mice with HT29 tumor xenografts to evaluate the effects of pazopanib, a small-molecule tyrosine kinase inhibitor selectively targeting VEGFR, PDGFR, and c-Kit. The changes in VEGFR imaging reflect a dramatic pazopanib-induced decrease in the number of VEGFR-2$^+$/CD31$^+$ endothelial cells (ECs) within the tumor vasculature followed by a relative increase in the number of ECs at the tumor edges [184].

The above mentioned data give us promising envisions as to the application of molecular imaging for therapy response monitoring. However, there are several issues need to be further explored. For example, integrins are not only overexpressed on tumor endothelial cells but also on tumor cells. In addition, there is heterogeneity of integrin expression between different tumors or even within the same tumor. In addition, tumor uptake and accumulation of imaging tracers is not only dependent on the receptor expression. Several other factors including vascular density and volume, vascular permeability and interstitial fluid pressure also affect the distribution [185,186]. All these factors will be changed after treatment, especially with anti-angiogenesis treatment.

CONCLUSIONS AND PERSPECTIVES

A multitude of imaging techniques is available for assessing tissue vasculature on a structural, functional and molecular level. A wide variety of targeting ligands (small molecules, peptidomimetics, peptides, and antibodies) have been conjugated with various imaging labels for MRI, ultrasound, optical, SPECT, PET, and multimodality imaging of angiogenesis. All these methods have been successfully used preclinically and will hopefully aid in antiangiogenic drug evaluation in animal studies. In the future, multimodality, multiplexing imaging will allow for evaluation of the angiogenic cascade in its full complexity to acquire comprehensive information. It is predictable that the new generation clinical PET/CT and preclinical microPET/microCT, as well as PET/MRI and microPET/microMRI currently in active development [187–189], will likely play a major role in molecular imaging of angiogenesis.

To further improve imaging of the angiogenesis process at molecular level, it is necessary to identify new angiogenesis related targets and corresponding specific ligands and to optimize currently available imaging probes. Thorough and full understanding of the physiological and pathological changes during angiogenesis will be critical for new target identification. Optimization of currently available imaging probes can be achieved by oligomerization (homo or hetero), glycosylation, PEGylation, and site-specific labeling, and so on. With all the efforts, molecular imaging techniques can bridge the gap between preclinical and clinical research to develop candidate drugs that have the optimal target specificity, pharmacokinetics, and efficacy. It is expected that in the foreseeable future, anigogenesis imaging will be routinely applied in anti-cancer clinical trials.

Acknowledgments

L. Zhu is partially supported by the scholarship from China Scholarship Council (CSC). G. Niu is an Imaging Sciences Training Fellowship jointly supported by the Radiology and Imaging Sciences Department, NIH Clinical Center and the Intramural Research Program, NIBIB, NIH. This research was supported by the Intramural Research Program of the NIBIB, NIH.

References

1. Folkman J. Angiogenesis in cancer, vascular, rheumatoid and other disease. Nat Med. 1995; 1:27–31. [PubMed: 7584949]

2. Bergers G, Benjamin LE. Tumorigenesis and the angiogenic switch. Nat Rev Cancer. 2003; 3:401–10. [PubMed: 12778130]
3. Carmeliet P. Angiogenesis in life, disease and medicine. Nature. 2005; 438:932–6. [PubMed: 16355210]
4. Folkman J, Watson K, Ingber D, Hanahan D. Induction of angiogenesis during the transition from hyperplasia to neoplasia. Nature. 1989; 339:58–61. [PubMed: 2469964]
5. Holash J, Maisonpierre PC, Compton D, Boland P, Alexander CR, Zagzag D, et al. Vessel cooption, regression, and growth in tumors mediated by angiopoietins and VEGF. Science. 1999; 284:1994–8. [PubMed: 10373119]
6. Folkman J. Tumor angiogenesis: therapeutic implications. N Engl J Med. 1971; 285:1182–6. [PubMed: 4938153]
7. Hanahan D, Folkman J. Patterns and emerging mechanisms of the angiogenic switch during tumorigenesis. Cell. 1996; 86:353–64. [PubMed: 8756718]
8. Arbiser JL, Moses MA, Fernandez CA, Ghiso N, Cao Y, Klauber N, et al. Oncogenic H-ras stimulates tumor angiogenesis by two distinct pathways. Proc Natl Acad Sci U S A. 1997; 94:861–6. [PubMed: 9023347]
9. Dameron KM, Volpert OV, Tainsky MA, Bouck N. Control of angiogenesis in fibroblasts by p53 regulation of thrombospondin-1. Science. 1994; 265:1582–4. [PubMed: 7521539]
10. Nguyen M. Angiogenic factors as tumor markers. Invest New Drugs. 1997; 15:29–37. [PubMed: 9195287]
11. Landgren E, Schiller P, Cao Y, Claesson-Welsh L. Placenta growth factor stimulates MAP kinase and mitogenicity but not phospholipase C-gamma and migration of endothelial cells expressing Flt 1. Oncogene. 1998; 16:359–67. [PubMed: 9467961]
12. Nor JE, Christensen J, Mooney DJ, Polverini PJ. Vascular endothelial growth factor (VEGF)-mediated angiogenesis is associated with enhanced endothelial cell survival and induction of Bcl-2 expression. Am J Pathol. 1999; 154:375–84. [PubMed: 10027396]
13. Paku S, Paweletz N. First steps of tumor-related angiogenesis. Lab Invest. 1991; 65:334–46. [PubMed: 1716330]
14. Hanahan D, Weinberg RA. The hallmarks of cancer. Cell. 2000; 100:57–70. [PubMed: 10647931]
15. Carmeliet P, Jain RK. Angiogenesis in cancer and other diseases. Nature. 2000; 407:249–57. [PubMed: 11001068]
16. Hillen F, Griffioen AW. Tumour vascularization: sprouting angiogenesis and beyond. Cancer Metastasis Rev. 2007; 26:489–502. [PubMed: 17717633]
17. Auguste P, Lemiere S, Larrieu-Lahargue F, Bikfalvi A. Molecular mechanisms of tumor vascularization. Crit Rev Oncol Hematol. 2005; 54:53–61. [PubMed: 15780907]
18. Kalluri R. Basement membranes: structure, assembly and role in tumour angiogenesis. Nat Rev Cancer. 2003; 3:422–33. [PubMed: 12778132]
19. Sang QX. Complex role of matrix metalloproteinases in angiogenesis. Cell Res. 1998; 8:171–7. [PubMed: 9791730]
20. Brooks PC, Clark RA, Cheresh DA. Requirement of vascular integrin $a_v b_3$ for angiogenesis. Science. 1994; 264:569–71. [PubMed: 7512751]
21. Friedlander M, Brooks PC, Shaffer RW, Kincaid CM, Varner JA, Cheresh DA. Definition of two angiogenic pathways by distinct alpha v integrins. Science. 1995; 270:1500–2. [PubMed: 7491498]
22. Gamble J, Meyer G, Noack L, Furze J, Matthias L, Kovach N, et al. B1 integrin activation inhibits in vitro tube formation: effects on cell migration, vacuole coalescence and lumen formation. Endothelium. 1999; 7:23–34. [PubMed: 10599558]
23. Jain RK. Normalization of tumor vasculature: an emerging concept in antiangiogenic therapy. Science. 2005; 307:58–62. [PubMed: 15637262]
24. Li JL, Sainson RC, Shi W, Leek R, Harrington LS, Preusser M, et al. Delta-like 4 Notch ligand regulates tumor angiogenesis, improves tumor vascular function, and promotes tumor growth in vivo. Cancer Res. 2007; 67:11244–53. [PubMed: 18056450]
25. Folkman J. Tumor angiogenesis and tissue factor. Nat Med. 1996; 2:167–8. [PubMed: 8574960]

26. Ferrara N. VEGF and the quest for tumour angiogenesis factors. Nat Rev Cancer. 2002; 2:795–803. [PubMed: 12360282]
27. Erjala K, Sundvall M, Junttila TT, Zhang N, Savisalo M, Mali P, et al. Signaling via ErbB2 and ErbB3 associates with resistance and epidermal growth factor receptor (EGFR) amplification with sensitivity to EGFR inhibitor gefitinib in head and neck squamous cell carcinoma cells. Clin Cancer Res. 2006; 12:4103–11. [PubMed: 16818711]
28. Watanabe H, Mamelak AJ, Wang B, Howell BG, Freed I, Esche C, et al. Anti-vascular endothelial growth factor receptor-2 (Flk-1/KDR) antibody suppresses contact hypersensitivity. Exp Dermatol. 2004; 13:671–81. [PubMed: 15500639]
29. Prewett M, Huber J, Li Y, Santiago A, O'Connor W, King K, et al. Antivascular endothelial growth factor receptor (fetal liver kinase 1) monoclonal antibody inhibits tumor angiogenesis and growth of several mouse and human tumors. Cancer Res. 1999; 59:5209–18. [PubMed: 10537299]
30. Ciardiello F, Caputo R, Damiano V, Troiani T, Vitagliano D, Carlomagno F, et al. Antitumor effects of ZD6474, a small molecule vascular endothelial growth factor receptor tyrosine kinase inhibitor, with additional activity against epidermal growth factor receptor tyrosine kinase. Clin Cancer Res. 2003; 9:1546–56. [PubMed: 12684431]
31. Wedge SR, Ogilvie DJ, Dukes M, Kendrew J, Curwen JO, Hennequin LF, et al. ZD4190: an orally active inhibitor of vascular endothelial growth factor signaling with broad-spectrum antitumor efficacy. Cancer Res. 2000; 60:970–5. [PubMed: 10706112]
32. Drevs J, Hofmann I, Hugenschmidt H, Wittig C, Madjar H, Muller M, et al. Effects of PTK787/ZK 222584, a specific inhibitor of vascular endothelial growth factor receptor tyrosine kinases, on primary tumor, metastasis, vessel density, and blood flow in a murine renal cell carcinoma model. Cancer Res. 2000; 60:4819–24. [PubMed: 10987292]
33. Bruns CJ, Liu W, Davis DW, Shaheen RM, McConkey DJ, Wilson MR, et al. Vascular endothelial growth factor is an in vivo survival factor for tumor endothelium in a murine model of colorectal carcinoma liver metastases. Cancer. 2000; 89:488–99. [PubMed: 10931447]
34. Laird AD, Christensen JG, Li G, Carver J, Smith K, Xin X, et al. SU6668 inhibits Flk-1/KDR and PDGFRbeta in vivo, resulting in rapid apoptosis of tumor vasculature and tumor regression in mice. Faseb J. 2002; 16:681–90. [PubMed: 11978732]
35. Presta LG, Chen H, O'Connor SJ, Chisholm V, Meng YG, Krummen L, et al. Humanization of an anti-vascular endothelial growth factor monoclonal antibody for the therapy of solid tumors and other disorders. Cancer Res. 1997; 57:4593–9. [PubMed: 9377574]
36. Faivre S, Djelloul S, Raymond E. New paradigms in anticancer therapy: targeting multiple signaling pathways with kinase inhibitors. Semin Oncol. 2006; 33:407–20. [PubMed: 16890796]
37. Ikezoe T, Nishioka C, Tasaka T, Yang Y, Komatsu N, Togitani K, et al. The antitumor effects of sunitinib (formerly SU11248) against a variety of human hematologic malignancies: enhancement of growth inhibition via inhibition of mammalian target of rapamycin signaling. Mol Cancer Ther. 2006; 5:2522–30. [PubMed: 17041096]
38. Willett CG, Boucher Y, di Tomaso E, Duda DG, Munn LL, Tong RT, et al. Direct evidence that the VEGF-specific antibody bevacizumab has antivascular effects in human rectal cancer. Nat Med. 2004; 10:145–7. [PubMed: 14745444]
39. Fujio Y, Walsh K. Akt mediates cytoprotection of endothelial cells by vascular endothelial growth factor in an anchorage-dependent manner. J Biol Chem. 1999; 274:16349–54. [PubMed: 10347193]
40. Hlatky L, Hahnfeldt P, Folkman J. Clinical application of antiangiogenic therapy: microvessel density, what it does and doesn't tell us. J Natl Cancer Inst. 2002; 94:883–93. [PubMed: 12072542]
41. Miller KD, Soule SE, Calley C, Emerson RE, Hutchins GD, Kopecky K, et al. Randomized phase II trial of the anti-angiogenic potential of doxorubicin and docetaxel; primary chemotherapy as Biomarker Discovery Laboratory. Breast Cancer Res Treat. 2005; 89:187–97. [PubMed: 15692762]
42. Hughes MS, Marsh JN, Zhang H, Woodson AK, Allen JS, Lacy EK, et al. Characterization of digital waveforms using thermodynamic analogs: detection of contrast-targeted tissue *in vivo*. IEEE Trans Ultrason Ferroelectr Freq Control. 2006; 53:1609–16. [PubMed: 16964911]

43. Li PC, Yang MJ. Transfer function analysis of ultrasonic time-intensity measurements. Ultrasound Med Biol. 2003; 29:1493–500. [PubMed: 14597347]
44. Wilhelm SM, Carter C, Tang L, Wilkie D, McNabola A, Rong H, et al. BAY 43-9006 exhibits broad spectrum oral antitumor activity and targets the RAF/MEK/ERK pathway and receptor tyrosine kinases involved in tumor progression and angiogenesis. Cancer Res. 2004; 64:7099–109. [PubMed: 15466206]
45. Padhani AR. MRI for assessing antivascular cancer treatments. Br J Radiol. 2003; 76(Spec No 1):S60–80. [PubMed: 15456715]
46. O'Connor JP, Jackson A, Parker GJ, Jayson GC. DCE-MRI biomarkers in the clinical evaluation of antiangiogenic and vascular disrupting agents. Br J Cancer. 2007; 96:189–95. [PubMed: 17211479]
47. Tozer GM. Measuring tumour vascular response to antivascular and antiangiogenic drugs. Br J Radiol. 2003; 76(Spec No 1):S23–35. [PubMed: 15456711]
48. Teicher BA, Emi Y, Kakeji Y, Northey D. TNP-470/minocycline/cytotoxic therapy: a systems approach to cancer therapy. Eur J Cancer. 1996; 32A:2461–6. [PubMed: 9059334]
49. Ratain MJ, Eckhardt SG. Phase II studies of modern drugs directed against new targets: if you are fazed, too, then resist. RECIST J Clin Oncol. 2004; 22:4442–5.
50. Yuan F, Chen Y, Dellian M, Safabakhsh N, Ferrara N, Jain RK. Time-dependent vascular regression and permeability changes in established human tumor xenografts induced by an anti-vascular endothelial growth factor/vascular permeability factor antibody. Proc Natl Acad Sci U S A. 1996; 93:14765–70. [PubMed: 8962129]
51. Massoud TF, Gambhir SS. Molecular imaging in living subjects: seeing fundamental biological processes in a new light. Genes Dev. 2003; 17:545–80. [PubMed: 12629038]
52. Nagengast WB, de Vries EG, Hospers GA, Mulder NH, de Jong JR, Hollema H, et al. In vivo VEGF imaging with radiolabeled bevacizumab in a human ovarian tumor xenograft. J Nucl Med. 2007; 48:1313–9. [PubMed: 17631557]
53. Collingridge DR, Carroll VA, Glaser M, Aboagye EO, Osman S, Hutchinson OC, et al. The development of [^{124}I]iodinated-VG76e: a novel tracer for imaging vascular endothelial growth factor *in vivo* using positron emission tomography. Cancer Res. 2002; 62:5912–9. [PubMed: 12384557]
54. Jayson GC, Zweit J, Jackson A, Mulatero C, Julyan P, Ranson M, et al. Molecular imaging and biological evaluation of HuMV833 anti-VEGF antibody: implications for trial design of antiangiogenic antibodies. J Natl Cancer Inst. 2002; 94:1484–93. [PubMed: 12359857]
55. Scheer MG, Stollman TH, Boerman OC, Verrijp K, Sweep FC, Leenders WP, et al. Imaging liver metastases of colorectal cancer patients with radiolabelled bevacizumab: Lack of correlation with VEGF-A expression. Eur J Cancer. 2008; 44:1835–40. [PubMed: 18632262]
56. Backer MV, Levashova Z, Patel V, Jehning BT, Claffey K, Blankenberg FG, et al. Molecular imaging of VEGF receptors in angiogenic vasculature with single-chain VEGF-based probes. Nat Med. 2007; 13:504–9. [PubMed: 17351626]
57. Cai W, Chen K, Mohamedali KA, Cao Q, Gambhir SS, Rosenblum MG, et al. PET of vascular endothelial growth factor receptor expression. J Nucl Med. 2006; 47:2048–56. [PubMed: 17138749]
58. Chen K, Cai W, Li ZB, Wang H, Chen X. Quantitative PET imaging of VEGF receptor expression. Mol Imaging Biol. 2009; 11:15–22. [PubMed: 18784964]
59. Lu E, Wagner WR, Schellenberger U, Abraham JA, Klibanov AL, Woulfe SR, et al. Targeted in vivo labeling of receptors for vascular endothelial growth factor: approach to identification of ischemic tissue. Circulation. 2003; 108:97–103. [PubMed: 12821549]
60. Blankenberg FG, Backer MV, Levashova Z, Patel V, Backer JM. In vivo tumor angiogenesis imaging with site-specific labeled (99m)Tc-HYNIC-VEGF. Eur J Nucl Med Mol Imaging. 2006; 33:841–8. [PubMed: 16699765]
61. Wang H, Chen K, Niu G, Chen X. Site-specifically biotinylated VEGF(121) for near-infrared fluorescence imaging of tumor angiogenesis. Mol Pharm. 2009; 6:285–94. [PubMed: 19099493]

62. Wang H, Cai W, Chen K, Li ZB, Kashefi A, He L, et al. A new PET tracer specific for vascular endothelial growth factor receptor 2. Eur J Nucl Med Mol Imaging. 2007; 34:2001–10. [PubMed: 17694307]
63. Cai W, Chen X. Anti-angiogenic cancer therapy based on integrin $a_v b_3$ antagonism. Anti-Cancer Agents Med Chem. 2006; 6:407–428.
64. Jia H, Jezequel S, Lohr M, Shaikh S, Davis D, Soker S, et al. Peptides encoded by exon 6 of VEGF inhibit endothelial cell biological responses and angiogenesis induced by VEGF. Biochem Biophys Res Commun. 2001; 283:164–73. [PubMed: 11322784]
65. Qin ZX, Li QW, Liu GY, Luo CX, Xie GF, Zheng L, et al. Imaging targeted at tumor with (188)Re-labeled VEGF(189) exon 6-encoded peptide and effects of the transfecting truncated KDR gene in tumor-bearing nude mice. Nucl Med Biol. 2009; 36:535–43. [PubMed: 19520294]
66. Korpanty G, Carbon JG, Grayburn PA, Fleming JB, Brekken RA. Monitoring response to anticancer therapy by targeting microbubbles to tumor vasculature. Clin Cancer Res. 2007; 13:323–30. [PubMed: 17200371]
67. Shohet RV, Chen S, Zhou YT, Wang Z, Meidell RS, Unger RH, et al. Echocardiographic destruction of albumin microbubbles directs gene delivery to the myocardium. Circulation. 2000; 101:2554–6. [PubMed: 10840004]
68. Underiner TL, Ruggeri B, Gingrich DE. Development of vascular endothelial growth factor receptor (VEGFR) kinase inhibitors as anti-angiogenic agents in cancer therapy. Curr Med Chem. 2004; 11:731–45. [PubMed: 15032727]
69. Willmann JK, Paulmurugan R, Chen K, Gheysens O, Rodriguez-Porcel M, Lutz AM, et al. US imaging of tumor angiogenesis with microbubbles targeted to vascular endothelial growth factor receptor type 2 in mice. Radiology. 2008; 246:508–18. [PubMed: 18180339]
70. Willmann JK, Cheng Z, Davis C, Lutz AM, Schipper ML, Nielsen CH, et al. Targeted microbubbles for imaging tumor angiogenesis: assessment of whole-body biodistribution with dynamic micro-PET in mice. Radiology. 2008; 249:212–9. [PubMed: 18695212]
71. Pochon S, Tardy I, Bussat P, Bettinger T, Brochot J, von Wronski M, et al. BR55: a lipopeptide-based VEGFR2-targeted ultrasound contrast agent for molecular imaging of angiogenesis. Invest Radiol. 45:89–95. [PubMed: 20027118]
72. Pillai R, Marinelli ER, Fan H, Nanjappan P, Song B, von Wronski MA, et al. A Phospholipid-PEG2000 Conjugate of a Vascular Endothelial Growth Factor Receptor 2 (VEGFR2)-Targeting Heterodimer Peptide for Contrast-Enhanced Ultrasound Imaging of Angiogenesis. Bioconjug Chem.
73. Izzo AD, Mackanos MA, Beckham JT, Jansen ED. *In vivo* optical imaging of expression of vascular endothelial growth factor following laser incision in skin Lasers. Surg Med. 2001; 29:343–50.
74. Lin PC. Optical imaging and tumor angiogenesis. J Cell Biochem. 2003; 90:484–91. [PubMed: 14523982]
75. Backer MV, Patel V, Jehning BT, Backer JM. Self-assembled “dock and lock” system for linking payloads to targeting proteins. Bioconjug Chem. 2006; 17:912–9. [PubMed: 16848397]
76. Backer MV, Gaynutdinov TI, Patel V, Bandyopadhyaya AK, Thirumamagal BT, Tjarks W, et al. Vascular endothelial growth factor selectively targets boronated dendrimers to tumor vasculature. Mol Cancer Ther. 2005; 4:1423–9. [PubMed: 16170035]
77. Chen K, Li ZB, Wang H, Cai W, Chen X. Dual-modality optical and positron emission tomography imaging of vascular endothelial growth factor receptor on tumor vasculature using quantum dots. Eur J Nucl Med Mol Imaging. 2008; 35:2235–44. [PubMed: 18566815]
78. Negrin RS, Contag CH. *In vivo* imaging using bioluminescence: a tool for probing graft-versus-host disease. Nat Rev Immunol. 2006; 6:484–90. [PubMed: 16724101]
79. Wang Y, Iyer M, Annala A, Wu L, Carey M, Gambhir SS. Noninvasive indirect imaging of vascular endothelial growth factor gene expression using bioluminescence imaging in living transgenic mice. Physiol Genomics. 2006; 24:173–80. [PubMed: 16410544]
80. Brooks PC, Montgomery AM, Rosenfeld M, Reisfeld RA, Hu T, Klier G, et al. Integrin alpha v beta 3 antagonists promote tumor regression by inducing apoptosis of angiogenic blood vessels. Cell. 1994; 79:1157–64. [PubMed: 7528107]

81. Cai W, Chen X. Multimodality molecular imaging of tumor angiogenesis. J Nucl Med. 2008; 49 (Suppl 2):113S–28S. [PubMed: 18523069]
82. Brakebusch C, Bouvard D, Stanchi F, Sakai T, Fassler R. Integrins in invasive growth. J Clin Invest. 2002; 109:999–1006. [PubMed: 11956235]
83. Hynes RO. Integrins: bidirectional, allosteric signaling machines. Cell. 2002; 110:673–87. [PubMed: 12297042]
84. Xiong JP, Stehle T, Zhang R, Joachimiak A, Frech M, Goodman SL, et al. Crystal structure of the extracellular segment of integrin $a_v b_3$ in complex with an Arg-Gly-Asp ligand. Science. 2002; 296:151–5. [PubMed: 11884718]
85. Ruoslahti E, Pierschbacher MD. New perspectives in cell adhesion: RGD and integrins. Science. 1987; 238:491–7. [PubMed: 2821619]
86. Jin H, Varner J. Integrins: roles in cancer development and as treatment targets. Br J Cancer. 2004; 90:561–565. [PubMed: 14760364]
87. Mizejewski GJ. Role of integrins in cancer: survey of expression patterns (44435). Proc Soc Exp Biol Med. 1999; 222:124–38. [PubMed: 10564536]
88. Brooks PC, Clark RA, Cheresh DA. Requirement of vascular integrin alpha v beta 3 for angiogenesis. Science. 1994; 264:569–71. [PubMed: 7512751]
89. Friedlander M, Theesfeld CL, Sugita M, Fruttiger M, Thomas MA, Chang S, et al. Involvement of integrins alpha v beta 3 and alpha v beta 5 in ocular neovascular diseases. Proc Natl Acad Sci U S A. 1996; 93:9764–9. [PubMed: 8790405]
90. Lu X, Lu D, Scully M, Kakkar V. The role of integrins in cancer and the development of anti-integrin therapeutic agents for cancer therapy. Perspect Medicin Chem. 2008; 2:57–73. [PubMed: 19787098]
91. Mousa SA. Anti-integrin as novel drug-discovery targets: potential therapeutic and diagnostic implications. Curr Opin Chem Biol. 2002; 6:534–41. [PubMed: 12133730]
92. Mullamitha SA, Ton NC, Parker GJ, Jackson A, Julyan PJ, Roberts C, et al. Phase I evaluation of a fully human anti-alphav integrin monoclonal antibody (CNTO 95) in patients with advanced solid tumors. Clin Cancer Res. 2007; 13:2128–35. [PubMed: 17404096]
93. Mitjans F, Meyer T, Fittschen C, Goodman S, Jonczyk A, Marshall JF, et al. In vivo therapy of malignant melanoma by means of antagonists of alphav integrins. Int J Cancer. 2000; 87:716–23. [PubMed: 10925366]
94. Dechantsreiter MA, Planker E, Matha B, Lohof E, Holzemann G, Jonczyk A, et al. N-Methylated cyclic RGD peptides as highly active and selective alpha(V)beta(3) integrin antagonists. J Med Chem. 1999; 42:3033–40. [PubMed: 10447947]
95. Belvisi L, Bernardi A, Colombo M, Manzoni L, Potenza D, Scolastico C, et al. Targeting integrins: insights into structure and activity of cyclic RGD pentapeptide mimics containing azabicycloalkane amino acids. Bioorg Med Chem. 2006; 14:169–80. [PubMed: 16214345]
96. Kumar CC, Malkowski M, Yin Z, Tanghetti E, Yaremko B, Nechuta T, et al. Inhibition of angiogenesis and tumor growth by SCH221153, a dual alpha(v)beta3 and alpha(v)beta5 integrin receptor antagonist. Cancer Res. 2001; 61:2232–8. [PubMed: 11280792]
97. Byron A, Humphries JD, Askari JA, Craig SE, Mould AP, Humphries MJ. Anti-integrin monoclonal antibodies. J Cell Sci. 2009; 122:4009–11. [PubMed: 19910492]
98. Haubner R, Wester HJ, Reuning U, Senekowitsch-Schmidtke R, Diefenbach B, Kessler H, et al. Radiolabeled alpha(v)beta3 integrin antagonists: a new class of tracers for tumor targeting. J Nucl Med. 1999; 40:1061–71. [PubMed: 10452325]
99. Haubner R, Wester HJ, Weber WA, Mang C, Ziegler SI, Goodman SL, et al. Noninvasive imaging of alpha(v)beta3 integrin expression using 18F-labeled RGD-containing glycopeptide and positron emission tomography. Cancer Res. 2001; 61:1781–5. [PubMed: 11280722]
100. Haubner R. Alphavbeta3-integrin imaging: a new approach to characterise angiogenesis? Eur J Nucl Med Mol Imaging. 2006; 33(Suppl 1):54–63. [PubMed: 16791598]
101. Harris JM, Martin NE, Modi M. Pegylation: a novel process for modifying pharmacokinetics. Clin Pharmacokinet. 2001; 40:539–51. [PubMed: 11510630]

102. Chen X, Park R, Shahinian AH, Bading JR, Conti PS. Pharmacokinetics and tumor retention of 125I-labeled RGD peptide are improved by PEGylation. Nucl Med Biol. 2004; 31:11–9. [PubMed: 14741566]
103. Noiri E, Goligorsky MS, Wang GJ, Wang J, Cabahug CJ, Sharma S, et al. Biodistribution and clearance of 99mTc-labeled Arg-Gly-Asp (RGD) peptide in rats with ischemic acute renal failure. J Am Soc Nephrol. 1996; 7:2682–8. [PubMed: 8989749]
104. Chen X, Hou Y, Tohme M, Park R, Khankaldyyan V, Gonzales-Gomez I, et al. Pegylated Arg-Gly-Asp peptide: 64Cu labeling and PET imaging of brain tumor alphavbeta3-integrin expression. J Nucl Med. 2004; 45:1776–83. [PubMed: 15471848]
105. Dijkgraaf I, Liu S, Kruijtzer JA, Soede AC, Oyen WJ, Liskamp RM, et al. Effects of linker variation on the in vitro and in vivo characteristics of an 111In-labeled RGD peptide. Nucl Med Biol. 2007; 34:29–35. [PubMed: 17210459]
106. Li ZB, Chen K, Chen X. (68)Ga-labeled multimeric RGD peptides for microPET imaging of integrin alpha(v)beta (3) expression. Eur J Nucl Med Mol Imaging. 2008; 35:1100–8. [PubMed: 18204838]
107. van Hagen PM, Breeman WA, Bernard HF, Schaar M, Mooij CM, Srinivasan A, et al. Evaluation of a radiolabelled cyclic DTPA-RGD analogue for tumour imaging and radionuclide therapy. Int J Cancer. 2000; 90:186–98. [PubMed: 10993959]
108. Bach-Gansmo T, Danielsson R, Saracco A, Wilczek B, Bogsrud TV, Fangberget A, et al. Integrin receptor imaging of breast cancer: a proof-of-concept study to evaluate 99mTc-NC100692. J Nucl Med. 2006; 47:1434–9. [PubMed: 16954550]
109. Kenny LM, Coombes RC, Oulie I, Contractor KB, Miller M, Spinks TJ, et al. Phase I trial of the positron-emitting Arg-Gly-Asp (RGD) peptide radioligand 18F-AH111585 in breast cancer patients. J Nucl Med. 2008; 49:879–86. [PubMed: 18483090]
110. Haubner R, Wester HJ, Burkhart F, Senekowitsch-Schmidtke R, Weber W, Goodman SL, et al. Glycosylated RGD-containing peptides: tracer for tumor targeting and angiogenesis imaging with improved biokinetics. J Nucl Med. 2001; 42:326–36. [PubMed: 11216533]
111. Haubner R, Kuhnast B, Mang C, Weber WA, Kessler H, Wester HJ, et al. [18F]Galacto-RGD: synthesis, radiolabeling, metabolic stability, and radiation dose estimates. Bioconjug Chem. 2004; 15:61–9. [PubMed: 14733584]
112. Haubner R, Weber WA, Beer AJ, Vabuliene E, Reim D, Sarbia M, et al. Noninvasive visualization of the activated alphavbeta3 integrin in cancer patients by positron emission tomography and [18F]Galacto-RGD. PLoS Med. 2005; 2:e70. [PubMed: 15783258]
113. Beer AJ, Haubner R, Goebel M, Luderschmidt S, Spilker ME, Wester HJ, et al. Biodistribution and pharmacokinetics of the alphavbeta3-selective tracer 18F-galacto-RGD in cancer patients. J Nucl Med. 2005; 46:1333–41. [PubMed: 16085591]
114. Beer AJ, Haubner R, Wolf I, Goebel M, Luderschmidt S, Niemeyer M, et al. PET-based human dosimetry of 18F-galacto-RGD, a new radiotracer for imaging alpha v beta3 expression. J Nucl Med. 2006; 47:763–9. [PubMed: 16644745]
115. Beer AJ, Haubner R, Sarbia M, Goebel M, Luderschmidt S, Grosu AL, et al. Positron emission tomography using [18F]Galacto-RGD identifies the level of integrin alpha(v)beta3 expression in man. Clin Cancer Res. 2006; 12:3942–9. [PubMed: 16818691]
116. Beer AJ, Lorenzen S, Metz S, Herrmann K, Watzlowik P, Wester HJ, et al. Comparison of integrin alphaVbeta3 expression and glucose metabolism in primary and metastatic lesions in cancer patients: a PET study using 18F-galacto-RGD and 18F-FDG. J Nucl Med. 2008; 49:22–9. [PubMed: 18077538]
117. Beer AJ, Grosu AL, Carlsen J, Kolk A, Sarbia M, Stangier I, et al. [18F]galacto-RGD positron emission tomography for imaging of alphavbeta3 expression on the neovasculature in patients with squamous cell carcinoma of the head and neck. Clin Cancer Res. 2007; 13:6610–6. [PubMed: 18006761]
118. Boturyn D, Coll JL, Garanger E, Favrot MC, Dumy P. Template assembled cyclopeptides as multimeric system for integrin targeting and endocytosis. J Am Chem Soc. 2004; 126:5730–9. [PubMed: 15125666]

119. Thumshirn G, Hersel U, Goodman SL, Kessler H. Multimeric cyclic RGD peptides as potential tools for tumor targeting: solid-phase peptide synthesis and chemoselective oxime ligation. Chemistry. 2003; 9:2717–25. [PubMed: 12772286]
120. Poethko T, Schottelius M, Thumshirn G, Hersel U, Herz M, Henriksen G, et al. Two-step methodology for high-yield routine radiohalogenation of peptides: (18)F-labeled RGD and octreotide analogs. J Nucl Med. 2004; 45:892–902. [PubMed: 15136641]
121. Chen X, Tohme M, Park R, Hou Y, Bading JR, Conti PS. Micro-PET imaging of alphavbeta3-integrin expression with 18F-labeled dimeric RGD peptide. Mol Imaging. 2004; 3:96–104. [PubMed: 15296674]
122. Zhang X, Xiong Z, Wu Y, Cai W, Tseng JR, Gambhir SS, et al. Quantitative PET imaging of tumor integrin alphavbeta3 expression with 18F-FRGD2. J Nucl Med. 2006; 47:113–21. [PubMed: 16391195]
123. Chen X, Park R, Tohme M, Shahinian AH, Bading JR, Conti PS. MicroPET and autoradiographic imaging of breast cancer alpha v-integrin expression using 18F-and 64Cu-labeled RGD peptide. Bioconjug Chem. 2004; 15:41–9. [PubMed: 14733582]
124. Chen X, Liu S, Hou Y, Tohme M, Park R, Bading JR, et al. MicroPET imaging of breast cancer alphav-integrin expression with 64Cu-labeled dimeric RGD peptides. Mol Imaging Biol. 2004; 6:350–9. [PubMed: 15380745]
125. Wu Z, Li ZB, Chen K, Cai W, He L, Chin FT, et al. microPET of tumor integrin alphavbeta3 expression using 18F-labeled PEGylated tetrameric RGD peptide (18F-FPRGD4). J Nucl Med. 2007; 48:1536–44. [PubMed: 17704249]
126. Li ZB, Cai W, Cao Q, Chen K, Wu Z, He L, et al. (64)Cu-labeled tetrameric and octameric RGD peptides for small-animal PET of tumor alpha(v)beta(3) integrin expression. J Nucl Med. 2007; 48:1162–71. [PubMed: 17574975]
127. Liu Z, Niu G, Shi J, Liu S, Wang F, Chen X. (68)Ga-labeled cyclic RGD dimers with Gly3 and PEG4 linkers: promising agents for tumor integrin alphavbeta3 PET imaging. Eur J Nucl Med Mol Imaging. 2009; 36:947–57. [PubMed: 19159928]
128. Liu Z, Liu S, Niu G, Wang F, Chen X. Optical imaging of integrin alphavbeta3 expression with near-infrared fluorescent RGD dimer with tetra(ethylene glycol) linkers. Mol Imaging. 2010; 9:21–9. [PubMed: 20128995]
129. Liu Z, Liu S, Wang F, Chen X. Noninvasive imaging of tumor integrin expression using (18)F-labeled RGD dimer peptide with PEG (4) linkers. Eur J Nucl Med Mol Imaging. 2009; 36:1296–307. [PubMed: 19296102]
130. Cai W, Wu Y, Chen K, Cao Q, Tice DA, Chen X. In vitro and in vivo characterization of 64Cu-labeled AbegrinTM, a humanized monoclonal antibody against integrin avb3. Cancer Res. 2006; 66:9673–81. [PubMed: 17018625]
131. Miao Z, Ren G, Liu H, Kimura RH, Jiang L, Cochran JR, et al. An engineered knottin peptide labeled with 18F for PET imaging of integrin expression. Bioconjug Chem. 2009; 20:2342–7. [PubMed: 19908826]
132. Kimura RH, Levin AM, Cochran FV, Cochran JR. Engineered cystine knot peptides that bind alphavbeta3, alphavbeta5, and alpha5beta1 integrins with low-nanomolar affinity. Proteins. 2009; 77:359–69. [PubMed: 19452550]
133. Kimura RH, Miao Z, Cheng Z, Gambhir SS, Cochran JR. A Dual-Labeled Knottin Peptide for PET and Near-Infrared Fluorescence Imaging of Integrin Expression in Living Subjects. Bioconjug Chem. 2010
134. Kimura RH, Miao Z, Cheng Z, Gambhir SS, Cochran JR. A Dual-Labeled Knottin Peptide for PET and Near-Infrared Fluorescence Imaging of Integrin Expression in Living Subjects. Bioconjug Chem.
135. Cai W, Chen K, Li ZB, Gambhir SS, Chen X. Dual-function probe for PET and near-infrared fluorescence imaging of tumor vasculature. J Nucl Med. 2007; 48:1862–70. [PubMed: 17942800]
136. Smith BR, Cheng Z, De A, Koh AL, Sinclair R, Gambhir SS. Real-time intravital imaging of RGD-quantum dot binding to luminal endothelium in mouse tumor neovasculature. Nano Lett. 2008; 8:2599–606. [PubMed: 18386933]

137. Lee HY, Li Z, Chen K, Hsu AR, Xu C, Xie J, et al. PET/MRI dual-modality tumor imaging using arginine-glycine-aspartic (RGD)-conjugated radiolabeled iron oxide nanoparticles. J Nucl Med. 2008; 49:1371–9. [PubMed: 18632815]
138. Xie J, Chen K, Lee HY, Xu C, Hsu AR, Peng S, et al. Ultrasmall c(RGDyK)-coated Fe3O4 nanoparticles and their specific targeting to integrin alpha(v)beta3-rich tumor cells. J Am Chem Soc. 2008; 130:7542–3. [PubMed: 18500805]
139. Chen K, Xie J, Xu H, Behera D, Michalski MH, Biswal S, et al. Triblock copolymer coated iron oxide nanoparticle conjugate for tumor integrin targeting. Biomaterials. 2009; 30:6912–9. [PubMed: 19773081]
140. Dayton PA, Pearson D, Clark J, Simon S, Schumann PA, Zutshi R, et al. Ultrasonic analysis of peptide- and antibody-targeted microbubble contrast agents for molecular imaging of alphavbeta3-expressing cells. Mol Imaging. 2004; 3:125–34. [PubMed: 15296677]
141. Willmann JK, Kimura RH, Deshpande N, Lutz AM, Cochran JR, Gambhir SS. Targeted contrast-enhanced ultrasound imaging of tumor angiogenesis with contrast microbubbles conjugated to integrin-binding knottin peptides. J Nucl Med. 51:433–40. [PubMed: 20150258]
142. Wagner S, Breyholz HJ, Faust A, Holtke C, Levkau B, Schober O, et al. Molecular imaging of matrix metalloproteinases in vivo using small molecule inhibitors for SPECT and PET. Curr Med Chem. 2006; 13:2819–38. [PubMed: 17073631]
143. Folgueras AR, Pendas AM, Sanchez LM, Lopez-Otin C. Matrix metalloproteinases in cancer: from new functions to improved inhibition strategies. Int J Dev Biol. 2004; 48:411–24. [PubMed: 15349816]
144. Park JH, Park SM, Park SH, Cho KH, Lee ST. Cleavage and functional loss of human apolipoprotein E by digestion of matrix metalloproteinase-14. Proteomics. 2008; 8:2926–35. [PubMed: 18655030]
145. Johnson JL, George SJ, Newby AC, Jackson CL. Divergent effects of matrix metalloproteinases 3, 7, 9, and 12 on atherosclerotic plaque stability in mouse brachiocephalic arteries. Proc Natl Acad Sci U S A. 2005; 102:15575–80. [PubMed: 16221765]
146. Heissig B, Hattori K, Friedrich M, Rafii S, Werb Z. Angiogenesis: vascular remodeling of the extracellular matrix involves metalloproteinases. Curr Opin Hematol. 2003; 10:136–41. [PubMed: 12579040]
147. Bellon G, Martiny L, Robinet A. Matrix metalloproteinases and matrikines in angiogenesis. Crit Rev Oncol Hematol. 2004; 49:203–20. [PubMed: 15036261]
148. Burbridge MF, Coge F, Galizzi JP, Boutin JA, West DC, Tucker GC. The role of the matrix metalloproteinases during in vitro vessel formation. Angiogenesis. 2002; 5:215–26. [PubMed: 12831062]
149. Haubner R. Noninvasive tracer techniques to characterize angiogenesis. Handb Exp Pharmacol. 2008:323–39. [PubMed: 18626609]
150. Li WP, Anderson CJ. Imaging matrix metalloproteinase expression in tumors. Q J Nucl Med. 2003; 47:201–8. [PubMed: 12897711]
151. Lee S, Park K, Kim K, Choi K, Kwon IC. Activatable imaging probes with amplified fluorescent signals. Chem Commun (Camb). 2008:4250–60. [PubMed: 18802536]
152. Lee S, Park K, Lee SY, Ryu JH, Park JW, Ahn HJ, et al. Dark quenched matrix metalloproteinase fluorogenic probe for imaging osteoarthritis development in vivo. Bioconjug Chem. 2008; 19:1743–7. [PubMed: 18729392]
153. Bremer C, Bredow S, Mahmood U, Weissleder R, Tung CH. Optical imaging of matrix metalloproteinase-2 activity in tumors: feasibility study in a mouse model. Radiology. 2001; 221:523–9. [PubMed: 11687699]
154. Jiang T, Olson ES, Nguyen QT, Roy M, Jennings PA, Tsien RY. Tumor imaging by means of proteolytic activation of cell-penetrating peptides. Proc Natl Acad Sci U S A. 2004; 101:17867–72. [PubMed: 15601762]
155. Olson ES, Aguilera TA, Jiang T, Ellies LG, Nguyen QT, Wong EH, et al. In vivo characterization of activatable cell penetrating peptides for targeting protease activity in cancer. Integr Biol (Camb). 2009; 1:382–93. [PubMed: 20023745]

156. Nguyen QT, Olson ES, Aguilera TA, Jiang T, Scadeng M, Ellies LG, et al. Surgery with molecular fluorescence imaging using activatable cell-penetrating peptides decreases residual cancer and improves survival. Proc Natl Acad Sci U S A. 107:4317–22. [PubMed: 20160097]
157. Yun CS, Javier A, Jennings T, Fisher M, Hira S, Peterson S, et al. Nanometal surface energy transfer in optical rulers, breaking the FRET barrier. J Am Chem Soc. 2005; 127:3115–9. [PubMed: 15740151]
158. Johansson MK, Cook RM, Xu J, Raymond KN. Time gating improves sensitivity in energy transfer assays with terbium chelate/dark quencher oligonucleotide probes. J Am Chem Soc. 2004; 126:16451–5. [PubMed: 15600347]
159. Lee S, Ryu JH, Park K, Lee A, Lee SY, Youn IC, et al. Polymeric nanoparticle-based activatable near-infrared nanosensor for protease determination in vivo. Nano Lett. 2009; 9:4412–6. [PubMed: 19842672]
160. Zhang Y, So MK, Rao J. Protease-modulated cellular uptake of quantum dots. Nano Lett. 2006; 6:1988–92. [PubMed: 16968013]
161. Xia Z, Xing Y, So MK, Koh AL, Sinclair R, Rao J. Multiplex detection of protease activity with quantum dot nanosensors prepared by intein-mediated specific bioconjugation. Anal Chem. 2008; 80:8649–55. [PubMed: 18922019]
162. Medina OP, Kairemo K, Valtanen H, Kangasniemi A, Kaukinen S, Ahonen I, et al. Radionuclide imaging of tumor xenografts in mice using a gelatinase-targeting peptide. Anticancer Res. 2005; 25:33–42. [PubMed: 15816516]
163. Hanaoka H, Mukai T, Habashita S, Asano D, Ogawa K, Kuroda Y, et al. Chemical design of a radiolabeled gelatinase inhibitor peptide for the imaging of gelatinase activity in tumors. Nucl Med Biol. 2007; 34:503–10. [PubMed: 17591550]
164. Sprague JE, Li WP, Liang K, Achilefu S, Anderson CJ. In vitro and in vivo investigation of matrix metalloproteinase expression in metastatic tumor models. Nucl Med Biol. 2006; 33:227–37. [PubMed: 16546677]
165. Zheng QH, Fei X, Liu X, Wang JQ, Bin Sun H, Mock BH, et al. Synthesis and preliminary biological evaluation of MMP inhibitor radiotracers [11C]methyl-halo-CGS 27023A analogs, new potential PET breast cancer imaging agents. Nucl Med Biol. 2002; 29:761–70. [PubMed: 12381456]
166. Furumoto S, Takashima K, Kubota K, Ido T, Iwata R, Fukuda H. Tumor detection using 18F-labeled matrix metalloproteinase-2 inhibitor. Nucl Med Biol. 2003; 30:119–25. [PubMed: 12623110]
167. Wagner S, Breyholz HJ, Law MP, Faust A, Holtke C, Schroer S, et al. Novel fluorinated derivatives of the broad-spectrum MMP inhibitors N-hydroxy-2(R)-[[(4-methoxyphenyl)sulfonyl](benzyl)- and (3-picolyl)-amino]-3-methyl-butanamide as potential tools for the molecular imaging of activated MMPs with PET. J Med Chem. 2007; 50:5752–64. [PubMed: 17956082]
168. Zheng QH, Fei X, Liu X, Wang JQ, Stone KL, Martinez TD, et al. Comparative studies of potential cancer biomarkers carbon-11 labeled MMP inhibitors (S)-2-(4′-[11C]methoxybiphenyl-4-sulfonylamino)-3-methylbutyric acid and N-hydroxy-(R)-2-[[(4′-[11C]methoxyphenyl)sulfonyl]benzylamino]-3-methylbut anamide. Nucl Med Biol. 2004; 31:77–85. [PubMed: 14741572]
169. Zheng QH, Fei X, DeGrado TR, Wang JQ, Stone KL, Martinez TD, et al. Synthesis, biodistribution and micro-PET imaging of a potential cancer biomarker carbon-11 labeled MMP inhibitor (2R)-2-[[4-(6-fluorohex-1-ynyl)phenyl]sulfonylamino]-3-methylbutyric acid [11C]methyl ester. Nucl Med Biol. 2003; 30:753–60. [PubMed: 14499334]
170. Kulasegaram R, Giersing B, Page CJ, Blower PJ, Williamson RA, Peters BS, et al. In vivo evaluation of 111In-DTPA-N-TIMP-2 in Kaposi sarcoma associated with HIV infection. Eur J Nucl Med. 2001; 28:756–61. [PubMed: 11440037]
171. Pirard B. Insight into the structural determinants for selective inhibition of matrix metalloproteinases. Drug Discov Today. 2007; 12:640–6. [PubMed: 17706545]
172. Niu G, Chen X. PET Imaging of Angiogenesis. PET Clin. 2009; 4:17–38. [PubMed: 20046926]

173. Rossin R, Berndorff D, Friebe M, Dinkelborg LM, Welch MJ. Small-animal PET of tumor angiogenesis using a (76)Br-labeled human recombinant antibody fragment to the ED-B domain of fibronectin. J Nucl Med. 2007; 48:1172–9. [PubMed: 17574989]

174. Tijink BM, Perk LR, Budde M, Stigter-van Walsum M, Visser GW, Kloet RW, et al. (124)I-L19-SIP for immuno-PET imaging of tumour vasculature and guidance of (131)I-L19-SIP radioimmunotherapy. Eur J Nucl Med Mol Imaging. 2009; 36:1235–44. [PubMed: 19259661]

175. Fonsatti E, Nicolay HJ, Altomonte M, Covre A, Maio M. Targeting cancer vasculature via endoglin/CD105: a novel antibody-based diagnostic and therapeutic strategy in solid tumours. Cardiovasc Res. 2009

176. Garrood T, Blades M, Haskard DO, Mather S, Pitzalis C. A novel model for the pre-clinical imaging of inflamed human synovial vasculature. Rheumatology (Oxford). 2009; 48:926–31. [PubMed: 19491304]

177. Currie MJ, Gunningham SP, Han C, Scott PA, Robinson BA, Harris AL, et al. Angiopoietin-1 is inversely related to thymidine phosphorylase expression in human breast cancer, indicating a role in vascular remodeling. Clin Cancer Res. 2001; 7:918–27. [PubMed: 11309342]

178. Seaman S, Stevens J, Yang MY, Logsdon D, Graff-Cherry C, St Croix B. Genes that distinguish physiological and pathological angiogenesis. Cancer Cell. 2007; 11:539–54. [PubMed: 17560335]

179. Yang AD, Bauer TW, Camp ER, Somcio R, Liu W, Fan F, et al. Improving delivery of antineoplastic agents with anti-vascular endothelial growth factor therapy. Cancer. 2005; 103:1561–70. [PubMed: 15754332]

180. Thomas AL, Morgan B, Horsfield MA, Higginson A, Kay A, Lee L, et al. Phase I study of the safety, tolerability, pharmacokinetics, and pharmacodynamics of PTK787/ZK 222584 administered twice daily in patients with advanced cancer. J Clin Oncol. 2005; 23:4162–71. [PubMed: 15867205]

181. Medved M, Karczmar G, Yang C, Dignam J, Gajewski TF, Kindler H, et al. Semiquantitative analysis of dynamic contrast enhanced MRI in cancer patients: Variability and changes in tumor tissue over time. J Magn Reson Imaging. 2004; 20:122–8. [PubMed: 15221817]

182. Morrison MS, Ricketts SA, Barnett J, Cuthbertson A, Tessier J, Wedge SR. Use of a novel Arg-Gly-Asp radioligand, 18F-AH111585, to determine changes in tumor vascularity after antitumor therapy. J Nucl Med. 2009; 50:116–22. [PubMed: 19091899]

183. Dumont RA, Hildebrandt I, Su H, Haubner R, Reischl G, Czernin JG, et al. Noninvasive imaging of alphaVbeta3 function as a predictor of the antimigratory and antiproliferative effects of dasatinib. Cancer Res. 2009; 69:3173–9. [PubMed: 19318569]

184. Blankenberg FG, Levashova Z, Sarkar SK, Pizzonia J, Backer MV, Backer JM. Noninvasive assessment of tumor VEGF receptors in response to treatment with pazopanib: a molecular imaging study. Transl Oncol. 2010; 3:56–64. [PubMed: 20165696]

185. Niu G, Li Z, Xie J, Le QT, Chen X. PET of EGFR antibody distribution in head and neck squamous cell carcinoma models. J Nucl Med. 2009; 50:1116–23. [PubMed: 19525473]

186. Niu G, Sun X, Cao Q, Courter D, Koong A, Le QT, et al. Cetuximab-based immunotherapy and radioimmunotherapy of head and neck squamous cell carcinoma. Clin Cancer Res. 2010; 16:2095–105. [PubMed: 20215534]

187. Shao Y, Cherry SR, Farahani K, Meadors K, Siegel S, Silverman RW, et al. Simultaneous PET and MR imaging. Phys Med Biol. 1997; 42:1965–70. [PubMed: 9364592]

188. Townsend DW, Beyer T. A combined PET/CT scanner: the path to true image fusion. Br J Radiol. 2002; 75(Spec No):S24–30. [PubMed: 12519732]

189. Catana C, Wu Y, Judenhofer MS, Qi J, Pichler BJ, Cherry SR. Simultaneous acquisition of multislice PET and MR images: initial results with a MR-compatible PET scanner. J Nucl Med. 2006; 47:1968–76. [PubMed: 17138739]

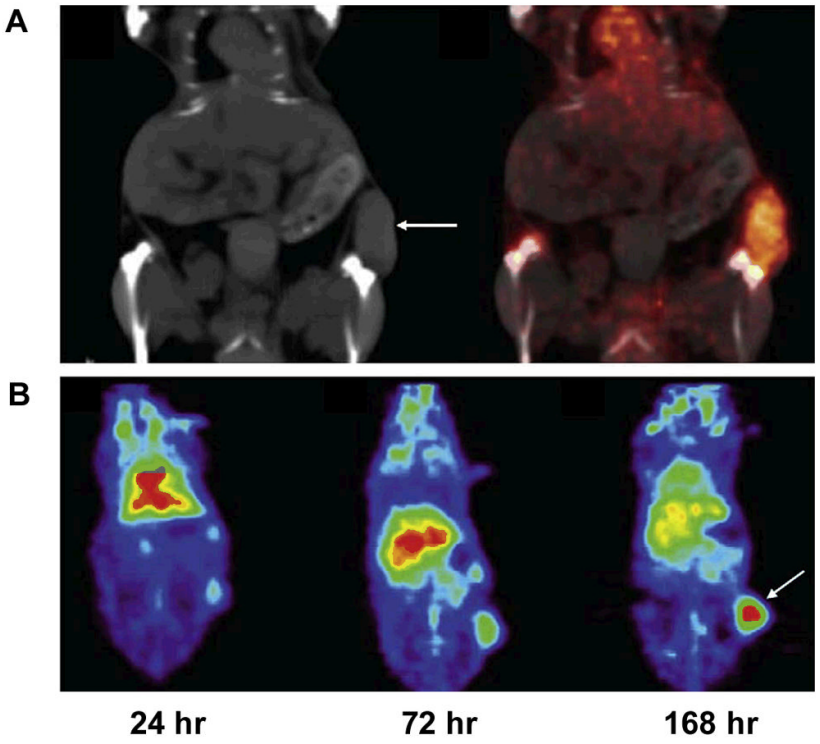

Figure 1.
Noninvasive imaging of VEGF expression *in vivo* by ^{89}Zr-labeled VEGF antibody Bevacizumab. **A.** Coronal CT image (left) with clear subcutaneous localization of SKOV-3 tumor (arrow) and fusion of microPET and CT images (right) (168 h after injection) (*arrows* indicate SKOV- 3 tumors). **B.** Coronal planes of microPET images at different time points after ^{89}Zr-Bevacizumab injection. Reproduced from reference [52] with permission.

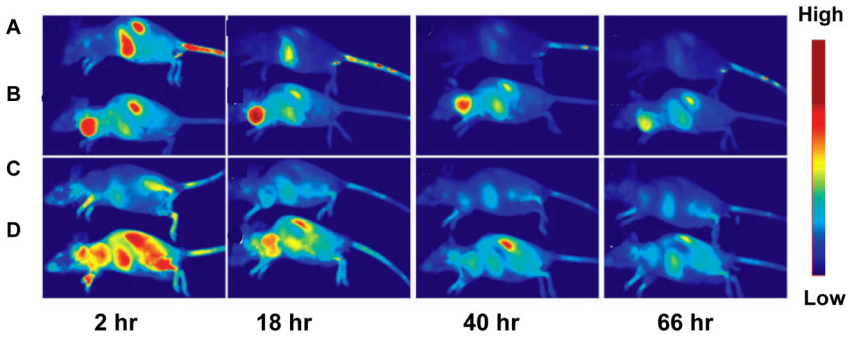

Figure 2.

In vivo optical imaging with site-specifically labeled $VEGF_{121}$. **A.** Optical image of 67NR tumors by $VEGF_{121}$-Avi-IRDye800 (VEGF-Avi/800) at different time point after tracer injection. **B.** Optical image of 67NR tumors by $VEGF_{121}$-Avi-biotin/streptavidin-IRDye800. **C.** Optical image of 67NR tumors by $VEGF_{mutant}$-Avi-biotin/streptavidin-IRDye800 (VEGFm-Avib/SA800). **D.** Optical image of 67NR tumors by streptavidin-IRDye800 (SA800). Reproduced from reference [61] with permission.

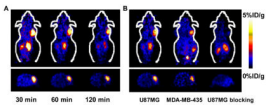

Figure 3.

MicroPET imaging of integrin expression using ^{18}F labeled RGD dimer peptide with PEG_4 linkers. **A.** Whole-body (top coronal, bottom transaxial) microPET images of U87MG tumor-bearing mice at different time points after injection of ^{18}F-FP-P-$PRGD_2$. **B.** MicroPET images at 60 min after injection of ^{18}F-FP-P-$PRGD_2$ in U87MG and MDA-MB-435 tumor-bearing mice without/with a blocking dose of c(RGDyK). Reproduced from reference [129] with permission.

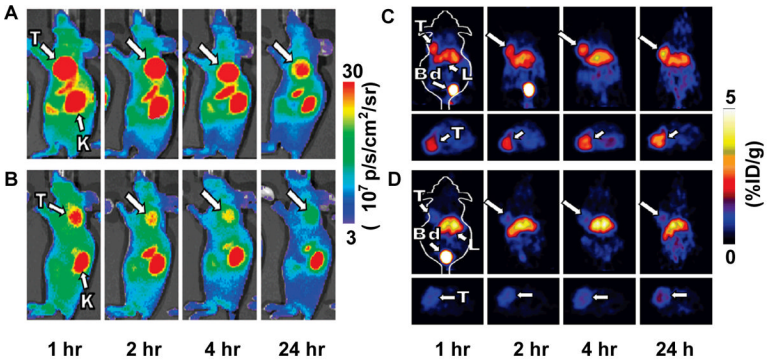

Figure 4.

Dual-labeled integrin-binding knottin peptide for microPET and NIRF imaging. **A.** MicroPET imaging of DOTA/Cy5.5-knottin peptide in mice bearing U87MG tumor. **B.** Mice were co-injected with an excess amount of unlabeled c(RGDyK) in addition to labeled knottin peptides as blocking experiment. **C.** NIRF imaging of DOTA/Cy5.5-knottin peptide in mice bearing U87MG tumor (*arrows* indicate U87MG tumors). **D.** Mice were co-injected with an excess amount of unlabeled c(RGDyK) in addition to labeled knottin peptides as blocking experiment. T, tumor; K, kidney; Bd, bladder; L, liver. Reproduced from reference [134] with permission.

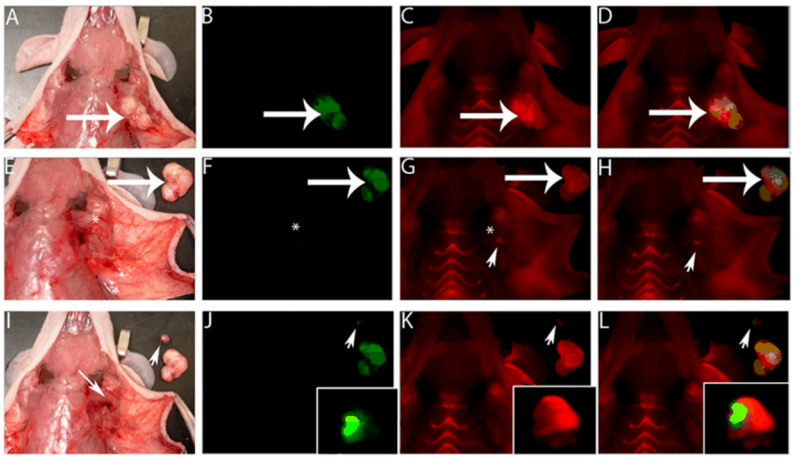

Figure 5.

ACPPs guide surgery. **A.** White light image of a MDA-MB-435 tumor-bearing mouse. **B.** Optical image of GFP-labeled tumor cells from the same mouse as in A (*arrow* indicate MDA-MB-435 tumor). **C.** Optical image of Cy5-labeled free ACPP in tumor. **D.** Colocalization of the Cy5 free ACPP with the GFP-labeled tumor. **E.** White light image of the excised tumor (large arrow) shown next to the mouse. **F.** Fluorescence imaging of the GFP signal in the tumor bed to confirm tumor excision successfully (*). **G and H.** Imaging of the Cy5 signal of tumor bed shows a residual fluorescence signal (arrowhead) in remaining tissue. **I.** A small piece of residual tumor (arrowhead) is excised (small arrow). **J and K.** Visualize of dissected tumor by GFP signal (J, arrowhead) and Cy5 free ACPP signal (K, arrowhead). **L.** Overlay GFP and Cy5 signal in dissected tumor. Reproduced from reference [156] with permission.